

1 Age constraints on intra-formational unconformities in Upper Jurassic-Lower Cretaceous carbonates
2 in northeast Turkey; geodynamic and hydrocarbon implications
3
4

5 Stephen J. Vincent^{1,*}, Li Guo¹, Rachel Flecker², Marcelle K. BouDagher-Fadel³, Robert M. Ellam⁴ &
6 Raif Kandemir⁵
7

8
9
10
11 ¹CASP, West Building, Madingley Rise, Madingley Road, Cambridge, CB3 0UD, UK
12 (stephen.vincent@casp.cam.ac.uk)
13
14

15
16 ²BRIDGE, School of Geographical Sciences and Cabot Institute, University of Bristol, University Road,
17 Bristol, BS8 1SS, UK (R.Flecker@bristol.ac.uk)
18
19

20
21 ³University College London, 2 Taviton Street, London WC1H 0BT, UK (m.fadel@ucl.ac.uk)
22

23
24 ⁴Scottish Universities Environmental Research Centre (SUERC), Scottish Enterprise Technology Park,
25 Rankine Ave., East Kilbride, G750QF, UK (Rob.Ellam@glasgow.ac.uk)
26
27

28 ⁵Recep Tayyip Erdoğan University, Department of Geological Engineering, 53000, Fener-Rize, Turkey
29 (raif.kandemir@erdogan.edu.tr)
30
31

32
33
34 *Corresponding author
35
36
37
38
39

40 Abstract

41
42
43 Upper Jurassic-lowermost Cretaceous carbonate build-ups are imaged on seismic data in the Black
44 Sea. They form important, untested, hydrocarbon reservoirs that are the focus of active exploration.
45
46 Outcrop analogues to these build-ups around the Black Sea contain a series of subaerial exposure
47 surfaces. The hiatuses associated with a number of these subaerial exposure surfaces have been
48 dated in a well exposed Callovian or Upper Oxfordian to Barremian shallow-water inner platform
49 carbonate succession (the Berdiga Formation) in the Eastern Pontides using strontium isotope
50 stratigraphy and foraminiferal biostratigraphy. They span the latest Kimmeridgian to Tithonian or
51 Berriasian, and the Hauterivian to Barremian. Less well constrained, but broadly contemporaneous
52
53
54
55
56
57
58
59
60
61
62
63
64
65

1 stratigraphic gaps in multiple successions around the Black Sea provide additional insights and point
2 to a regional driving mechanism. The timing of hiatus formation does not correspond to periods of
3
4 eustatic lowstand. It does coincide, however, with Late Tithonian to Berriasian and Hauterivian to
5
6 Early Aptian episodes of rifting in the Greater Caucasus Basin, located farther to the north. Thus, it is
7
8 possible that subaerial exposure was caused by rift flank uplift during periods of regional extension.
9
10 Uplift due to slab break off is discounted as a control because it post-dates (rather than pre-dates)
11
12 locally developed Kimmeridgian magmatism. Rift-flank uplift is likely to have also affected carbonate
13
14 build-ups on the intervening rift shoulders to the eastern Black Sea, the Shatskiy Ridge and the Mid
15
16 Black Sea High. At outcrop, subaerial exposure is often associated with karstification and secondary
17
18 porosity development. Similar processes may have occurred in the offshore helping to enhance the
19
20 reservoir quality of these exploration targets.
21
22
23
24
25
26
27
28
29

30 Keywords: Black Sea, Berdiga Formation, strontium isotope stratigraphy, Pontides, reservoir
31
32 potential
33
34
35
36
37
38

39 1 Introduction

40
41

42 Hydrocarbons hosted in Tethyan Upper Jurassic reef build-ups form a major resource, with their
43
44 potential exemplified by the South Yolotan–Osman (Galkynysh) field in the Amu-Dar’ya Basin,
45
46 Turkmenistan. This field hosts the world’s second largest gas reserves estimated to be between
47
48 13.1 trillion and 21.2 trillion cubic meters of gas in place (Gaffney, Cline and Associates, 2011 audit).
49
50

51
52 Seismic reflection data in the Black Sea appear to show a number of possible carbonate build-ups
53
54 along the Shatskiy Ridge, eastern Black Sea (Nikishin et al., 2015b). Regional considerations would
55
56 suggest that they are of Late Jurassic-earliest Cretaceous age. The build-ups are up to 1-2 km thick,
57
58 75 km long and 25 km wide (Afanasenkov et al., 2005, 2007). They are deeply buried (~2.5-7 km;
59
60
61
62
63
64
65

1 Meisner et al., 2009), at water depths typically greater than 2 km and are the focus of on-going
2 exploration activity. Until they are penetrated by boreholes and the results released, we are reliant
3
4 on outcrop data from Upper Jurassic-lowermost Cretaceous carbonate rocks around the margins of
5
6 the Black Sea to provide insights into the nature of these offshore exploration targets.
7
8

9
10 We have carried out extensive work on these outcrop analogues (e.g. Guo et al., 2011). Observed
11
12 porosities are typically less than 5%. However, at a number of key outcrops in the Pontides (Turkey),
13
14 the western Greater Caucasus (Russia) and Crimea (disputed), erosive surfaces that display evidence
15
16 for subaerial exposure have been observed (e.g. Figure 4 of Guo et al., 2011). Some of these are
17
18 associated with karstification and secondary porosity development. This may have enhanced the
19
20 reservoir characteristics of these carbonate units in the subsurface and have formed
21
22 intraformational markers that can be identified on seismic sections.
23
24

25
26
27 Insufficient age diagnostic fauna are present within the shallow-marine carbonate outcrop
28
29 analogues to determine accurately the age of these subaerial exposure surfaces. As a result, it is
30
31 unclear whether they are synchronous. This uncertainty impacts upon our ability to predict their
32
33 presence in the subsurface of the Black Sea basin.
34
35
36

37
38 This study is the first step towards addressing the paucity of age control and utilises strontium
39
40 isotope stratigraphy combined with foraminiferal biostratigraphy. These techniques have been used
41
42 to constrain the age of a relatively well-exposed Upper Jurassic-Lower Cretaceous carbonate-
43
44 dominated platform-interior succession (locality PT09_21) in the Eastern Pontides, Turkey, which
45
46 contains a number of surfaces that display evidence for subaerial exposure and / or erosion.
47
48
49

50 51 52 53 54 2 Geological background

55
56
57 Upper Jurassic to Lower Cretaceous strata at locality PT09_21 crop out between the villages of Kale
58
59 and Nazlıçayır in the region of Gümüşhane, NE Turkey, in the Eastern Pontides. Geologically, the
60
61
62
63
64
65

1 region forms part of eastern Sakarya Zone, which is bounded by the Black Sea to the north and the
2 İzmir-Ankara-Erzincan and Sevan-Akera sutures to the south (Figure 1). These sutures represent the
3
4 former position of the northern Neotethys Ocean that closed due to northerly-directed subduction
5
6 during Late Cretaceous to Eocene time (Okay and Şahintürk, 1997; Robertson et al., 2014; Robertson
7
8 and Dixon, 1984; Şengör and Yılmaz, 1981). Closure resulted in the development of a series of mostly
9
10 south-dipping, north-vergent thrust sheets in the south, whilst a more autochthonous region is
11
12 preserved to the north.
13
14

15
16
17 The basement of the eastern Sakarya Zone comprises a pre-Upper Carboniferous high-grade
18
19 metamorphic complex (the Pular Massif) intruded by Carboniferous-Permian granitoids (Okay, 1996;
20
21 Okay and Şahintürk, 1997; Topuz et al., 2004a; Topuz et al., 2004b; Topuz et al., 2007; Topuz et al.,
22
23 2010). In the eastern Sakarya Zone, these are locally overlain by a thick Upper Carboniferous-Lower
24
25 Permian shallow-marine to non-marine sedimentary sequence (Okay and Leven, 1996). Lastly,
26
27 Permo-Triassic metabasite-marble-phyllite units are exposed in the Ağvanis and Tokat massifs (Okay
28
29 and Şahintürk, 1997). Together these rocks are generally considered to represent the products of
30
31 their Variscan accretion to Laurasia and the subsequent northward subduction of Paleotethys
32
33 beneath this margin (Kazmin, 2006; Okay and Şahintürk, 1997; Okay and Topuz, 2017; Robinson et
34
35 al., 1995).
36
37
38
39
40

41
42 Lower to Middle Jurassic strata unconformably overlie older rocks. They were deposited in an
43
44 extensional setting and are up to 2240 m thick. In the study region they are known as the Şenköy
45
46 Formation (Kandemir, 2004). Broadly speaking they form a transgressive-regressive succession
47
48 comprised of basal alluvial conglomerates and sandstones, shallow-marine sandstones and possibly
49
50 *Ammonitico Rosso* condensed carbonates, volcanic and volcanoclastic gravity flow deposits (that
51
52 make up the majority of the succession) and, in places, an upper interval of coal- and gypsum-
53
54 bearing siliciclastic rocks (Görür et al., 1983; Kandemir, 2004; Kandemir and Yılmaz, 2009; Koçyiğit
55
56 and Altınar, 2002; Okay and Şahintürk, 1997; Yılmaz, 2002). Facies typically become finer grained
57
58
59
60
61
62
63
64
65

1 and deeper marine towards the south (Okay and Şahintürk, 1997). Extension is attributed to roll-
2 back during either the southerly subduction of Paleotethys to the north of the Sakarya continent
3
4 (Dokuz et al., 2017; Dokuz et al., 2010; Görür et al., 1983; Koçyiğit and Altiner, 2002; Şengör and
5
6 Yılmaz, 1981; Tüysüz, 1990; Yılmaz et al., 1997) or the northerly subduction of Neotethys to its south
7
8
9 (Kaz'min and Tikhonova, 2006; Okay et al., 2014; Ustaömer and Robertson, 2010).

10
11
12 Relative tectonic quiescence (Okay and Nikishin, 2015), combined with a eustatic sea-level rise and
13
14 climatic amelioration (Kiessling et al., 1999; Leinfelder et al., 2002), resulted in a switch to
15
16 carbonate-dominated sedimentation in the eastern Sakarya Zone during Late Jurassic (or possibly
17
18 latest Middle Jurassic) to Early Cretaceous time. This is reflected in the deposition of the up to
19
20 1000 m thick Berdiga Formation (Pelin, 1977) or Berdiga Limestone (Kırmacı et al., 1996). In the
21
22 northern, autochthonous region, this unit formed a south-facing carbonate platform that is the focus
23
24 of this study. Deeper-water sediments were deposited in what was to become the allochthonous
25
26 zone to the south.
27
28
29
30

31
32 Volcanic and volcanoclastic intercalations are present in the Upper Jurassic-lowermost Cretaceous
33
34 successions of the western Sakarya Zone (Altiner et al., 1991), the eastern Sakarya Zone (Dokuz et
35
36 al., 2017; Konak et al., 2009; Ustaömer and Robertson, 2010) and the northern Transcaucasus
37
38 (Adamia et al., 1992; Kazmin et al., 1986). The lavas in the eastern Sakarya Zone were probably
39
40 generated in a within-plate setting (Dokuz et al., 2017; Ustaömer and Robertson, 2010).
41
42
43
44
45
46
47

48 3 Previous work on the Berdiga Formation

49
50

51
52 The Berdiga Formation has been studied by numerous authors (e.g. Kırmacı, 1992; Kırmacı et al.,
53
54 1996; Koch et al., 2008; Koçyiğit and Altiner, 2002; Taslı et al., 1999; Yılmaz, 1992). The age of the
55
56 unit, however, remains poorly constrained, in large part due to a paucity of biostratigraphic marker
57
58 species. In the autochthonous northern region, for instance, authors have variously suggested that
59
60
61
62
63
64
65

1 sedimentation commenced in the Aalenian-Bajocian (Pelin, 1977), Callovian (Kırmacı, 1992;
2 Robinson et al., 1995), Oxfordian (Koch et al., 2008) or Kimmeridgian (Dokuz and Tanyolu, 2006; Taslı
3 et al., 1999). Callovian-aged detrital zircons in the underlying Şenköy Formation (Akdoğan et al.,
4 submitted) close to the Berdiga Formation type section near Alucra, more precisely constrain a
5 Callovian or younger depositional onset age for the formation in this region.
6
7
8
9
10

11 Rifting disrupted sedimentation on the Berdiga carbonate platform during Cretaceous time (Eren
12 and Taslı, 2002; Konak et al., 2009; Taslı et al., 1999; Yılmaz, 2002; Yılmaz and Kandemir, 2006). This
13 resulted in erosion, karstification or hardground formation on the highs, and a deepening and
14 change in carbonate facies in subsiding regions. On the highs, sedimentation typically continued
15 until the Late Barremian (Pelin, 1977) or Early Aptian (Eren and Taslı, 2002). In the lows, deeper
16 water carbonate-dominated sedimentation may have continued until the Turonian (Eren and Taslı,
17 2002; Taslı et al., 1999; Taslı and Özsayar, 1997).
18
19
20
21
22
23
24
25
26
27
28
29

30 A number of studies of the Berdiga Formation have been carried out in the vicinity of locality
31 PT09_21 (Eren and Taslı, 2002; Kara-Gülbay et al., 2012; Kırmacı et al., 1996; Koch et al., 2008). Here
32 the formation is estimated to be up to 590 m thick (Eren, 1983). The majority of these studies
33 focussed on the upper part of the formation and a possibly lacustrine, bituminous interval or its
34 contact with overlying units. Only the study by Koch et al. (2008) documented the lower ~320 m of
35 the formation (although not its basal contact). They subdivided the formation into 15 units and
36 described the facies and diagenesis of the succession in great detail in outcrops which they termed
37 the Kircaova section.
38
39
40
41
42
43
44
45
46
47
48
49

50 We revisited the Kircaova section (our locality PT09_21E; Figure 2). The main aims of our study were
51 to document the presence of a major erosional disconformity within the lower part of the section
52 not recognised by Koch *et al.* (2008), constrain better the age of the section based on additional
53 biostratigraphic and strontium isotopic determinations, and highlight the potential regional
54 significance of this (and younger) disconformity surfaces. Our study was not designed to replicate
55
56
57
58
59
60
61
62
63
64
65

1 the facies and diagenetic aspects of Koch et al. (2008), although we have complemented it with
2 some additional field and microscopic observations. The nature of the succession is described below
3
4 and summarised in Table 1.
5
6
7
8
9

10 4 Stratigraphy and facies

11
12 The Kircaova section runs between 40.34506°N, 39.72918°E and 40.34837°N, 39.73112°E (locality
13 PT09_21E) (Figure 1). The base of the Berdiga Formation is not exposed in this section but was
14 observed at locality PT09_21A (40.38020°N, 39.67691°E) (Figure 3). Here, presumed Middle Jurassic
15 volcaniclastic sediments of the Şenköy Formation are unconformably overlain by a pebbly limestone
16 containing volcaniclastic and granitic clasts, followed by medium-bedded arenaceous limestones and
17 thin-bedded sandstones and silty mudstones. These lithologies are poorly exposed and
18 approximately 6 m thick.
19
20
21
22
23
24
25
26
27
28
29
30

31 Koch et al. (2008) subdivided the lowermost part of the Berdiga Formation into 3 units beneath a
32 prominent lava flow (unit IV; Table 1; Figure 4) that forms a regional marker (Figure 2 and Figure 3).
33

34 We augmented observations in this part of the Kircaova section with those at locality PT09_21B
35 (40.36089°N, 39.68825°E to 40.35525°N, 39.69027°E) along a tributary of the Keçi River (Figure 3).
36

37 The thickness of units I-III are taken from Koch et al. (2008). Sample positions are located on
38 Figure 4.
39
40
41
42
43
44
45

46 Unit I is 18 m thick and consists mainly of very thick-bedded intraclastic packstones-grainstones
47 (sample 21B_09) and intraclastic-bioclastic grainstones (sample 21B_08) deposited on a shallow-
48 water, moderate- to high-energy platform interior (Table 1). Coated grains (oncoids) are abundant in
49 the lower part of the unit. Benthic foraminifera (both large and small), gastropods, bivalves and
50 corals have been recognised; locally *Tubiphytes* fragments are present. High faunal diversity was also
51 documented by Koch et al. (2008).
52
53
54
55
56
57
58
59
60
61
62
63
64
65

1
2
3
4
5
6
7
8
9
10
11
12
13
14
15
16
17
18
19
20
21
22
23
24
25
26
27
28
29
30
31
32
33
34
35
36
37
38
39
40
41
42
43
44
45
46
47
48
49
50
51
52
53
54
55
56
57
58
59
60
61
62
63
64
65

Unit II is 29 m thick and is dominated by medium- to thick-bedded dolostones (samples 21B_07 and 21B_06). The original textures of many dolostones are obscured. Some dolostones show ghost textures of grainstones with bioclasts, lithoclasts and ooids, as well as matrix-rich peloidal and lithoclastic packstones that lack bioclasts (Koch et al., 2008). Koch et al. (2008) suggested that this unit was mainly deposited in a restricted platform interior during decreased energy levels, interrupted by episodes of open and higher energy conditions.

Unit III is 23 m thick and comprises mainly medium- to thick-bedded dolostones in the lower part (sample 21B_05) and lime mudstones in the upper part (sample 21E_01) (Table 1). They contain traces of benthic foraminifera and other bioclasts and were continuously formed in a restricted shallow-marine platform interior (Koch et al., 2008). Traces of volcanic rock fragments indicate the presence of contemporaneous volcanic activity (Koch et al., 2008). A gastropod floatstone with meteoric dissolution and cementation features occurs near the top of the unit at locality PT09_21E (sample 21E_02; Figure 5A).

Unit IV is 10 m thick and dominated by a highly weathered doleritic lava flow with plagioclase phenocrysts and calcite amygdales (samples 21B_01 and 21E_03) (Table 1; Figure 4). Pillow structures, entrained rafts of contorted limestone (sample 21B_04) and breccia lenses suggest subaqueous eruption. Our Ar-Ar dating of plagioclase crystals from this unit yielded an erroneously young (Aptian) age, most likely due to argon loss because of the altered nature of the material. The top of the unit is capped by greenish tuffaceous siltstones and reddish silty mudstones that were likely deposited in near shore or subaerial environments. This unit has previously been referred to as the Olivine dolerite sill (Tokel, 1972), Diabase member (Eren, 1983), Keçidere basalt (Taslı, 1997), Diabase sill (Koch et al., 2008) or part of the Kuşakkaya Member (Dokuz et al., 2017).

Unit V is up to 54 m thick and comprises a cliff-forming interval of thick-bedded lime mudstones (samples 21B_02, 21B_03, 21E_10, 21E_11 and 21E_12) (Figure 2, Figure 5B and Figure 6A-B). It likely represents deposition in a low energy, restricted shallow-water environment. Altered volcanic

1 rock fragments have also been documented (Koch et al., 2008). The top of unit V is marked by a
2 pronounced erosion surface with up to 45 m of local relief (Figure 2, Figure 4 and Figure 6A-B). Along
3
4 the edge of this incised valley, the underlying limestones are brecciated (Figure 6C) and cut by
5
6 fissures and cracks that are filled with brownish and greenish clays. It is likely that the erosion
7
8 surface was formed during subaerial exposure. Koch et al. (2008) did not identify this surface.
9

10
11
12 Above the disconformity surface, the subdivisions of Koch et al. (2008) are less distinctive. Unit VI is
13
14 up to ~62 m thick. Initial, incised valley filling sediments consist mainly of the following: limestone
15
16 breccias; fine-grained conglomerates; scoured, laminated, cross-laminated and cross-bedded
17
18 sandstones; lime mudstones; and dolostones with laminated structures (e.g. samples 21E_04 to
19
20 21E_06) (Figure 4). Abundant quartz, angular limestone and volcanic clasts are present. Sandstone
21
22 sample 21E_04 is a volcanic lithic arkose, presumably reflecting the nearby erosion of unit IV or its
23
24 equivalents. The upper part of unit VI on the shoulder of the incised valley comprises poorly
25
26 exposed, medium- to thick-bedded dolostones (samples 21E_07 and 21E_08) (Figure 2, Figure 4 and
27
28 Figure 6A-B). This part of the unit was also recorded by Koch et al. (2008) who documented lime
29
30 mudstones with traces of ostracods, which could represent deposition in a low energy, restricted
31
32 shallow-water environment.
33
34
35
36
37

38
39 Unit VII is 57 m thick and poorly exposed. The base of the unit is marked by dolostones with
40
41 abundant quartz granules. Upward, further dolostones are exposed (samples 21E_13 and 21E_14;
42
43 Figure 5C); some contain ghost textures of peloids and intraclasts (sample 21E_09). Ghost textures
44
45 of molluscs and echinoids have been described by Koch et al. (2008) who suggested that this unit
46
47 was formed in a more open shallow-marine environment with high energy conditions.
48
49
50

51
52 Unit VIII is 5 m thick and comprises well exposed medium- to thick-bedded intraclastic and bioclastic,
53
54 coated grain packstones and grainstones with abundant foraminifera (samples 21E_15 to 21E_17)
55
56 (Figure 2 and Figure 5D). This unit represents deposition in a high energy, open shallow-water
57
58 environment.
59
60
61
62
63
64
65

1 Unit IX is 30 m thick and is dominated by well exposed medium- to thick-bedded, dolomitised
2 bioclastic wackestones (samples 21E_18 to 21E_20) (Figure 4). These were probably deposited in low
3
4 to moderate water energy conditions.
5
6

7 Units X-XII are ~57 m thick and only poorly to moderately exposed (Figure 2 and Figure 4). They
8
9 comprise medium- to thick-bedded intraclastic and bioclastic wackestones, packstones and
10
11 grainstones (e.g. Figure 5E) that have undergone differing amounts of dolomitisation (samples
12
13 21E_21 to 21E_23).
14
15
16

17 The top of the logged succession forms prominent cliffs (Figure 2). Units XIII-XIV are ~24 m thick and
18
19 are characterised by three prominent erosion surfaces (B-D) that are each overlain by reddened
20
21 breccio-conglomerates composed predominantly of limestone clasts (Figure 4 and Figure 6D-G).
22
23 Erosion surface C separates limestones cut by fissures filled with clays, below, from carbonate clasts
24
25 that are cemented in a meniscus style above (Figure 5F). Koch et al. (2008) also mentioned mud
26
27 cracks and soils associated with these erosion surfaces. The remainder of the interval comprises a
28
29 wide variety of lithologies including sandstone, foraminifera packstone-grainstone, mollusc
30
31 floatstone, intraclastic and bioclastic grainstone, bioclastic wackestone, lime mudstones and
32
33 laminated stromatolites (e.g. samples 21E_24 to 21E_30) indicative of varying energy, shallow-water
34
35 conditions. Koch et al. (2008) reported an increased presence of volcanic rock fragments and quartz
36
37 grains.
38
39
40
41
42
43
44

45 Unit XV is at least 19 m thick and comprises thick-bedded bioclastic packstones and grainstones with
46
47 minor lime mudstone interbeds (samples 21E_31 to 21E_33). Algal laminations and large bivalves
48
49 are evident and Koch et al. (2008) recorded local birdseye structures suggesting a shallow, possibly
50
51 intertidal, environment.
52
53
54
55
56
57
58
59
60
61
62
63
64
65

1 We did not record data from Koch et al. (2008)'s final unit XVI. According to these authors it is 23 m
2 thick and comprises interbeds of intraclastic, foraminiferal wackestones, packstones and
3
4 grainstones.
5
6
7
8
9

10 5 Diagenesis

11
12 The main diagenetic processes in the Berdiga Formation are micritisation, cementation,
13
14 karstification, dissolution, compaction and dolomitisation. Micritisation resulted in the formation of
15
16 micritic envelopes around original grains and is common in intraclastic bioclastic grainstones in the
17
18 Kircaova section (Figure 5A). Cementation resulted in different generations of cements that are
19
20 irregularly developed. Early formed isopachous cements line cavities in intraclastic-oid and
21
22 intraclastic-bioclastic grainstones (Figure 5D). Drusy mosaic (Figure 5D), blocky spar and poikilotopic
23
24 cements commonly fill the remaining pore space. Pendant and meniscus cements are typically
25
26 formed due to gravitation in meteoric-vadose environments (Figure 5A, F). Karstification was
27
28 observed beneath the lava flow and erosion surfaces A to C. Dissolution vugs filled with blocky
29
30 calcite cements occur locally. Intense dolomitisation is pervasively developed throughout much of
31
32 the succession. Dolomites contain early formed fine-grained subhedral dolomite crystals (Figure 5C)
33
34 and, in places, coarse-grained, late replacive, rhombohedra (Figure 5B). Additional diagenetic details
35
36 can be found in Koch et al. (2008).
37
38
39
40
41
42
43
44
45
46
47
48

49 6 Age control

50 6.1 Microfauna

51
52 No age diagnostic macrofauna were observed in the field. Instead multiple thin sections were made
53
54 for each of the samples and these were examined using a transmitted light petrological-type
55
56
57
58
59
60
61
62
63
64
65

1 microscope in order that their micropaleontological components could be identified. The results are
2 presented as Table 2, with key forms illustrated in Figure 7. The age of diagnostic assemblages,
3 based on BouDagher-Fadel (2008, 2012, 2015), are consistent with their stratigraphic position and
4 range from Bathonian-Oxfordian to Late Barremian-Aptian (Figure 4).
5
6
7
8
9

10 11 12 13 6.2 Strontium isotope stratigraphy 14

15 16 17 6.2.1 Sampling strategy 18

19
20 The Sr isotope ratio of ocean water has varied throughout earth history and has been calibrated to
21 provide a powerful chronostratigraphic tool (e.g. McArthur et al., 2001). The method relies on
22 biogenic carbonate preserving the $^{87}\text{Sr}/^{86}\text{Sr}$ of marine water (Burke et al., 1982; Elderfield, 1986).
23
24 Secondary alteration can however result in Sr isotope ratios that reflect either freshwater run-off or
25 pore water chemistry. Consequently, it is important to target and analyse only carbonate where
26 there is no evidence of post-depositional diagenesis. Some studies advocate trace element
27 geochemistry to identify samples that have enhanced concentration of e.g. Fe and Mn through
28 diagenetic alteration that can be excluded from strontium isotope stratigraphy (e.g. Denison et al.,
29 1994; Kuznetsov et al., 2012). While trace element composition undoubtedly has a role in identifying
30 diagenetic alteration, especially when attempting to reconstruct seawater $^{87}\text{Sr}/^{86}\text{Sr}$ using whole-rock
31 limestones (e.g. Denison et al., 1994), it is unclear whether these specific criteria are robust for
32 samples of differing geological age and/or sedimentary environment. In this study we prefer to
33 assess diagenesis by petrographic examination and exclude altered material by careful micro-
34 sampling.
35
36
37
38
39
40
41
42
43
44
45
46
47
48
49
50
51

52
53
54 Samples were thin sectioned, stained for calcite and dolomite and inspected under a polarising
55 microscope. Carbonate shells with well-preserved micro-structure and areas of biogenic lime mud
56 were identified on the thin section and then highlighted on the rock chip from which the thin section
57
58
59
60
61
62
63
64
65

1 had been made. A micro-drill was used to generate carbonate powder from the highlighted area
2 with a typical sample spot size of ~2 mm. Every attempt was made to avoid material likely to have
3 undergone diagenetic alteration, for instance aragonitic or high-Mg calcite shells with poor
4 microstructure preservation, dolomite or carbonate veins. In some instances, however, it was not
5 possible to be sure that only primary biogenic carbonate was sampled as drilling occurs out of the
6 plane of the thin section.
7
8
9

10
11
12
13
14 Samples were leached in 1N ammonium acetate (Gorokhov et al., 1995) and then dissolved in 2.5 M
15 HCl. Residual Sr/silicate impurities were rejected by centrifugation. Sr was separated using SrSpec®
16 resin (Eichrom Technologies LLC). Samples were loaded onto Re filaments with a Ta₂O₅ activator and
17 measured on a VG Sector 54-30 mass spectrometer in dynamic multi-collection mode. Mass
18 fractionation was corrected using the exponential law and $^{86}\text{Sr}/^{88}\text{Sr} = 0.1194$. During the course of
19 this study NIST SRM987 gave $^{87}\text{Sr}/^{86}\text{Sr} = 0.710260 \pm 0.000018$ (2σ) which is within error of the
20 consensus SRM987 value (0.710248) suggested by McArthur et al. (2001). To be entirely consistent
21 with this consensus value our data could be adjusted by (0.710248/0.710260) but we have not
22 applied such a correction because we do not seek to misrepresent the uncertainty inherent in the Sr
23 isotope method.
24
25
26
27
28
29
30
31
32
33
34
35
36
37
38
39
40
41
42

43 6.2.2 Results

44
45
46 Nineteen samples were analysed for their Sr isotope ratio (Table 3). When compared with the Sr
47 isotope seawater curve (McArthur et al., 2012), these values correspond to multiple possible ages
48 because the curve varies considerably through this period of the Mesozoic (Figure 8, insert).
49 However, biostratigraphic information from the section (Table 2) provides constraints on which of
50 these ages are mostly likely to correspond to the Sr isotope ratio measured. In addition, stratigraphic
51 integrity must be maintained and this also excludes some possible age interpretations of the
52
53
54
55
56
57
58
59
60
61
62
63
64
65

1 $^{87}\text{Sr}/^{86}\text{Sr}$ values (Table 3). Of the nineteen samples analysed, sixteen provide ages that are
2 compatible with both these constraints and indicate a stratigraphic section spanning the Callovian or
3
4 Oxfordian to Barremian, a period of c. 35 Ma (Figure 4). This suggests that the Sr isotope ratios
5 measured reflect the primary Sr isotope ratio of coeval seawater and consequently provide robust
6
7 age constraints on the section. Absolute age values are taken from Gradstein et al. (2012).
8
9

10
11
12 Samples 21B_08, 21E_02, 21B_03, 21E_05, 21E_06, 21E_14, 21E_17 and 21E_23 are relatively
13 straightforward to interpret because they are consistent with the biostratigraphic information and
14
15 preserve stratigraphic integrity (Table 3). Nine samples are slightly more complicated to interpret
16
17 and are discussed below.
18
19
20

21
22
23 Samples HUR8 and 21B_09 were collected stratigraphically ~4 m apart. Their Sr isotope ratios are
24
25 within analytical error of each other and lie close to a minima on the Sr isotope seawater curve, such
26
27 that two age ranges are possible; 166-164 Ma (Early to Middle Callovian) and 160-155 Ma (Middle
28
29 Oxfordian to Early Kimmeridgian) (Table 3 & Figure 4). Foraminiferal constraints from samples within
30
31 this part of the section suggest that it is no younger than Oxfordian in age.
32
33
34

35
36 Sample 21E_11 has a slightly higher Sr isotope ratio than overlying sample 21E_12. This is also the
37
38 case for sample 21E_27 relative to overlying sample 21E_29. Given the increasing Sr isotopic ratio
39
40 values with decreasing age on the Kimmeridgian to Hauterivian limb of the Sr isotope seawater
41
42 curve (Figure 8), these samples appear to be in the wrong stratigraphic order. However, the Sr
43
44 isotopic values of both pairs of samples are within analytical error, such that ages common to both
45
46 are permissible and further restrict their likely age ranges (Figure 4).
47
48
49

50
51 Two analyses were taken from sample 21E_30, one from a rudist shell and another from the micritic
52
53 infill of that shell. Both samples are within error of each other, but yielded strontium ratios that are
54
55 higher than the best estimate of oceanic values in the Early Cretaceous (Figure 8). The $^{87}\text{Sr}/^{86}\text{Sr}$ for
56
57 the rudist lies within the Sr isotope seawater curve uncertainty, while only the analytical error for
58
59
60
61
62
63
64
65

1 the micritic sample overlaps with the top of the uncertainty on the Sr isotope seawater curve. The
2 age of this sample is therefore estimated as being at the highest point of the Early Cretaceous
3 strontium curve (Figure 8), but its exact age should be treated with caution.
4
5

6
7 Sample PT09_SV_021E_32 was sampled close to a carbonate vein (Table 3), but in this instance the
8 Sr ratio measured corresponds with an age compatible with biostratigraphic constraints and relative
9 stratigraphic position. However, the age of this sample should be treated with caution.
10
11

12
13 Three samples, HUR9, 21B_08 and 21E_028, yielded Sr isotope ratios incompatible with their
14 stratigraphic relationship to other dated samples and with foraminiferal biostratigraphic constraints.
15 In the case of 21B_08, this is likely to be the result of including some diagenetic Sr from an adjacent
16 carbonate vein (Table 3). Although we attempted to sample dense micritic elements within samples
17 HUR9 and 21E_28, it is also possible that they included some diagenetic Sr from diffuse dissolution
18 voids.
19
20
21
22
23
24
25
26
27
28
29
30
31
32

33 34 6.3 Discussion 35

36
37 The top of the Berdiga Formation was not sampled in this study and therefore the age of the
38 formation range cannot be constrained. However, our Sr and biostratigraphic analysis indicates that
39 it must span from at least c. 158 Ma to c. 127 Ma (Late Oxfordian - Late Barremian; Figure 4 and
40 Figure 9a) at this locality. The base of the section could be Callovian in age.
41
42
43
44
45

46
47 Within the lower part of the succession, there appears to be an increase in carbonate sedimentation
48 rate from between ~5-41 m/Ma in units I-III to above 43 m/Ma in unit V above the lava flow
49 (Figure 4). The lava flow itself is probably Late Kimmeridgian in age. This is younger than the
50 estimates of Taslı (1997) (Late Oxfordian-Early Kimmeridgian) and Koch et al. (2008) (Middle
51 Kimmeridgian). Dokuz et al. (2017) dated the lava flow to between 155-150 Ma (Late Kimmeridgian-
52 Early Tithonian) based on the fossil data of Koch et al. (2008); it is unclear whether the difference in
53
54
55
56
57
58
59
60
61
62
63
64
65

1 reported age between these sources results from the reinterpretation of species ranges or simply
2 the use of a chronostratigraphic scheme other than Gradstein et al. (2012).
3

4
5 The age range of missing strata at the pronounced disconformity at the top of unit V (Figure 2), as
6
7
8
9
10
11
12
13
14
15
16
17
18
19
20
21
22
23
24
25
26
27
28
29
30
31
32
33
34
35
36
37
38
39
40
41
42
43
44
45
46
47
48
49
50
51
52
53
54
55
56
57
58
59
60
61
62
63
64
65

The age range of missing strata at the pronounced disconformity at the top of unit V (Figure 2), as constrained by samples 21E_11 and 21E_12, and sample 21E_05, spans 9-13 million years from the very latest Kimmeridgian to somewhere in the Berriasian (Figure 4 and Figure 9a). However, because sample 21E_05 was not collected from the base of the incised valley fill, the age gap will have been shorter. Extrapolation of sedimentation rates suggests that sedimentation could have resumed by the latest Tithonian.

Sedimentation rates in units VI-XII above the lower disconformity surface (A) have increased with time from between ~5-18 m/Ma to above 102 m/Ma (Figure 4). This is likely to reflect intermittent high-energy conditions and sediment bypassing within the incised valley, followed by more continuous sedimentation and carbonate production during the re-establishment of the carbonate platform in overlying units.

The 3 hiatuses and intervening sediments within units XIII-XIV occur within an interval spanning between 3-6 million years during the Hauterivian to Barremian (Figure 4 and Figure 9a). Sedimentation rates in the upper part of unit XIV and XV appear to have been relatively slow. This is similar to the situation above erosion surface A and is probably a result of bypass / intermittent erosion as reflected in the relatively coarse-grained, high-energy nature of these sediments.

7 Insights from other Black Sea outcrops

Insights into the significance of, and controls on, hiatus formation in the Eastern Pontides, can be gained by reviewing the location and age of other Upper Jurassic to Lower Cretaceous successions in the Black Sea region (Figure 9).

1 In the Central Pontides, we examined a section south of Küre at locality PT09_017 (41.70450°N,
2 33.69394°E; Figure 1 and Figure 9b). Its basement comprises Upper Triassic phyllites intruded by the
3
4 Ađlı Porphyry that yielded a 154 ± 2 Ma Rb-Sr cooling age (Aydın et al., 1995). This constrains the
5
6 maximum depositional age of overlying basal conglomerates (locally known as the Bürnük
7
8 Formation) that pass gradationally up into up to ~80 m of shallow-water carbonates of the İnaltı
9
10 Formation. The İnaltı and Berdiga formations are roughly age equivalent (Figure 9). The carbonates
11
12 are overlain by conglomerates of the Çađlayan Formation via a disconformity that has a local
13
14 incisional relief of ~50 m. Similar stratigraphic patterns have been observed elsewhere in the Central
15
16 Pontides (Derman and İztan, 1997; Kaya and Altıner, 2015; Okay et al., 2017) (Figure 9c). Our
17
18 biostratigraphic determinations from locality PT09_017 indicate a Kimmeridgian-Tithonian age range
19
20 for the carbonate succession (Table 4). In addition, a single strontium isotope ratio measured from 5
21
22 m below the top of the İnaltı Formation (sample 17_15) yields a value (0.707211 ± 0.000026) that
23
24 equates to an Early Berriasian age (145.05-142.05 Ma) and constrains the minimum age of carbonate
25
26 deposition (Figure 9b). This is consistent with the Kimmeridgian to Early Berriasian biostratigraphic
27
28 ages for the İnaltı Formation obtained from similar outcrops in the Central Pontides by Okay et al.
29
30 (2017) (Figure 9c). Analysis of a microbial overgrowth in the overlying conglomeratic Çađlayan
31
32 Formation yielded a strontium isotope value (0.708037 ± 0.000036) incompatible with the age of the
33
34 underlying sediments. The work of Okay et al. (2017) would suggest that the Çađlayan Formation is
35
36 probably mid Barremian or younger in age (Figure 9c) and therefore equivalent to sediments
37
38 deposited above erosion surface D at Kırcaova (Figure 9a).
39
40
41
42
43
44
45
46
47

48 Observations from the Central Pontides highlight two things. Firstly, carbonate deposition continued
49
50 through the Tithonian and into the Early Berriasian (Figure 9b, c). If the same were true for the
51
52 Eastern Pontides, this would suggest that much of the hiatus associated with erosion surface A at
53
54 Kırcaova resulted from the post-depositional erosion of uppermost Kimmeridgian to Lower
55
56 Berriasian strata rather than from non-deposition. Secondly, sediments equivalent to those
57
58 deposited between erosion surfaces A and D at Kırcaova have not yet been recognised (Figure 9).
59
60
61
62
63
64
65

1
2
3
4
5
6
7
8
9
10
11
12
13
14
15
16
17
18
19
20
21
22
23
24
25
26
27
28
29
30
31
32
33
34
35
36
37
38
39
40
41
42
43
44
45
46
47
48
49
50
51
52
53
54
55
56
57
58
59
60
61
62
63
64
65

Either (i) the Central Pontides was a region of uplift and non-deposition during this time period (Okay et al., 2017), (ii) sediments were removed by later relative base-level falls equivalent to those responsible for erosion surfaces B-D at Kırcaova or (iii) sediments, potentially similar to the İncigez Formation developed farther west (see below; Figure 9d), are present but have yet to be recognised.

In the İstanbul Zone of the Western Pontides, we examined a section around Zonguldak at locality PT09_003 (41.42279°N, 31.73215°E; Figure 1 and Figure 9d). As in the Central Pontides, carbonate-dominated sediments overlie a conglomerate-draped unconformity. These carbonates were originally also named the İnaltı Formation and mapped to be Late Jurassic to Early Cretaceous in age (Ketin and Gümüş, 1963). Subsequent mapping, however, identified an important disconformity separating Kimmeridgian to Berriasian carbonates from undated overlying continental red beds that fill an irregular topography (Derman and İztan, 1997; Derman and Sayılı, 1995). These are overlain by further carbonates of Late Barremian-earliest Aptian age (Masse et al., 2009). Based on these observations, the İnalti Formation was redefined to form only the lower part of this carbonate sequence (Derman and İztan, 1997; Derman and Sayılı, 1995). The red beds were named the İncigez Formation and the upper carbonate sequence, the Öküşmedere Formation (Figure 9d).

Observations from the Western Pontides highlight four things. Firstly, the major disconformity developed here may have been triggered by the same relative base-level fall responsible for erosion surface A at Kırcaova. Secondly, the barren İncigez Formation represents sedimentation between erosion surfaces A and D. Derman and İztan (1997, their figure 2) originally placed this formation in the uppermost Valanginian to Hauterivian (Figure 9d). However, if the same sedimentary responses are common across the Pontides, our work would suggest that this unit is likely to be equivalent to the Berriasian to Valanginian incised valley fill of unit VI at Kırcaova (Figure 4 and Figure 9a). Thirdly, the Upper Barremian to lowermost Aptian Öküşmedere Formation, like the Çağlayan Formation, represents sediment time equivalent to those deposited above erosion surface D at Kırcaova (Figure 9d). Fourthly, if the disconformity surfaces observed at Kırcaova can be documented to be of

1 mappable extent then, just as has happened in the Western Pontides, it would be good stratigraphic
2 practise to rename the individual components here to reflect their genetic disconnection, with the
3
4 Berdiga Formation term being restricted to Jurassic strata only.
5
6

7
8 Given that most tectonic models propose that Black Sea oceanic spreading occurred sometime in the
9
10 Cretaceous to Eocene (e.g. Görür, 1988; Kazmin et al., 2000; Nikishin et al., 2015a; Okay et al., 2013),
11
12 the Caucasus and Crimea would have been broadly contiguous with the Eastern Pontides during Late
13
14 Jurassic-Early Cretaceous carbonate deposition. Observations from these regions are therefore also
15
16 considered below.
17
18

19
20 The only strontium isotope stratigraphy studies published on similarly-aged carbonate platform
21
22 sediments in the Black Sea region are from the Baydar region of southwest Crimea (Rud'ko et al.,
23
24 2017) and the Demerdzhi Plateau in central Crimea (Rud'ko et al., 2014). Both of these studies
25
26 yielded 6 reliable $^{87}\text{Sr}/^{86}\text{Sr}$ values from carbonate platform facies of the Yalta Formation and imply
27
28 c. 153.7-151.8 Ma and c. 153.1-148.8 Ma (Late Kimmeridgian to Early Tithonian) age ranges,
29
30 respectively (Figure 9e, g). As in the Central and Western Pontides, this indicates that carbonate
31
32 deposition was on-going during the period represented by hiatus A at Kircaova.
33
34
35

36
37
38 Rud'ko et al. (2017) also dated part of the overlying Baydar Formation in the Baydar region to be
39
40 Early Berriasian in age (Figure 9e). It comprises carbonate breccias which they interpreted as the
41
42 sedimentary response to a regional (?erosive) event at the Jurassic-Cretaceous boundary. The
43
44 formation was previously thought to be Late Tithonian in age (Chaykovskiy et al., 2006) (Figure 9f),
45
46 however, and an Upper Tithonian element is permitted by the strontium isotope data and by the
47
48 fact that they did not sample the base of the formation. Thus the change to brecciated facies may
49
50 have occurred in Late Tithonian time. A disconformity has not been documented at the base or
51
52 within the Upper Tithonian Bedenekyr Formation at Demerdzhi (Figure 9h). However, it does contain
53
54 interbeds of sandstone and conglomerate that might conceivably occur above such a hiatal surface.
55
56
57
58
59
60
61
62
63
64
65

1 In summary, observations from southwest and central Crimea might provide evidence for Late
2 Tithonian disconformity formation. However, when compared with the more robust evidence for an
3 Early Berriasian hiatus above the Bedenekyr Formation in central Crimea (Fikolina et al., 2008)
4 (Figure 9h) and a major tectonic event between the Baydar Formation and Early Cretaceous
5 mudstones in southwest Crimea (Chaykovskiy et al., 2006) this is thought, at best, to be secondary to
6 an intra-Berriasian relative base-level fall. This interpretation is consistent with observations from a
7 number of other regions in Crimea and from the Russian western Greater Caucasus, where Tithonian
8 or Lower Berriasian platform carbonates or evaporates are disconformably overlain by mid/Upper
9 Berriasian or younger sediments (e.g. Bucur et al., 2014; Guo et al., 2011; Korsakov et al., 2004;
10 Korsakov et al., 2002; Nikishin et al., 2015c; Vincent et al., 2016) (Figure 9h-i). Given that
11 sedimentation was also re-established at Kircaova sometime during the latest Tithonian to
12 Berriasian, it is possible that a broadly contemporaneous Berriasian relative base-level fall may have
13 been responsible for all of the approximate Jurassic-Cretaceous boundary stratigraphic gaps
14 discussed above (Figure 9).
15
16
17
18
19
20
21
22
23
24
25
26
27
28
29
30
31

32
33
34 Mid/Upper Berriasian to Valanginian sedimentation, largely absent in the Central and Western
35 Pontides, occurred in the western Greater Caucasus and Crimea, as it did in the Eastern Pontides
36 (Figure 9). Individual Hauterivian to Lower Barremian formations in central Crimea are bound by
37 disconformities (Figure 9h), whilst a Late Hauterivian to Early Barremian hiatus occurs in strata in
38 southwest Crimea (Figure 9f). The Upper Hauterivian to Barremian Gubs Formation in the northern
39 western Greater Caucasus also disconformably overlies older strata (Figure 9i). Thus while it is not
40 possible to correlate specific events with those responsible for erosion surfaces B to D at Kircaova, a
41 general phase of discontinuous sedimentation is apparent. Lower Aptian strata are absent from all of
42 the Crimean and Caucasus examples highlighted in this study (Figure 9).
43
44
45
46
47
48
49
50
51
52
53

54 55 56 57 58 59 8 Regional implications and conclusions 60 61 62 63 64 65

1 This study successfully applies strontium isotope stratigraphy to Upper Jurassic-Lower Cretaceous
2 carbonate rocks in the Eastern Pontides for the first time. The combined biostratigraphic and Sr
3
4 isotope constraints provide greater stratigraphic resolution that was previously available from
5
6 biostratigraphy alone.
7
8
9

10 The study indicates that Upper Jurassic-Lower Cretaceous carbonate deposition in the Gümüşhane
11 region of the Eastern Pontides spanned at least the Late Oxfordian to Late Barremian (c. 158-
12
13 127 Ma). The base of the section may be Callovian in age. Carbonate deposition was interrupted by
14
15 volcanism during the Late Kimmeridgian, although the presence of volcanic material in underlying
16
17 sediments (unit III; Koch et al., 2008) suggests that volcanism may have commenced regionally in the
18
19 Early Kimmeridgian. The hiatus associated with the pronounced incisional surface in the lower part
20
21 of the succession (erosion surface A) is latest Kimmeridgian to Tithonian or Berriasian in age.
22
23 Multiple erosion surfaces (B-D) in the upper part of the Kırcaova section were formed sometime
24
25 during the Hauterivian to Barremian. Meteoric dissolution and karstification is associated with the
26
27 lava flow and erosion surfaces A to C (Figure 5A, F).
28
29
30
31
32
33

34 Multiple fluctuations in sea level per stage within the Late Jurassic and Early Cretaceous mean that it
35
36 is theoretically possible to match each of the relative base-level falls recognised in this study with
37
38 eustasy (Figure 9). However, the mismatch in the ages of the hiatuses recognised in this study and
39
40 longer term falls in sea level during the Late Tithonian and, particularly, during the Late Barremian to
41
42 Early Valanginian (Haq, 2014) (Figure 9) indicate that eustasy was not the main driving mechanism
43
44 for their formation and that, instead, tectonic controls were probably the driver of relative base-
45
46 level change.
47
48
49
50

51 Dokuz et al. (2017) attributed disconformity formation at erosion surface A at Kırcaova to rebound
52
53 following slab breakoff after the Cimmerian closure of Paleotethys. This explanation is problematic
54
55 because this would require (1) the southerly subduction of Paleotethys, north of the eastern Sakarya
56
57 Zone, and (2) a time lag of at least c. 1-3.5 million years and potentially as much as c. 10-16 million
58
59
60
61
62
63
64
65

1 years between magmatism (which began during deposition of unit III) and relative base-level fall. As
2 Dokuz et al. (2017) conceded, not all tectonic models incorporate southerly subduction and
3
4 Cimmerian continental collision (e.g. Golonka, 2004; Okay, 2000; Okay and Nikishin, 2015; Pickett
5
6 and Robertson, 2004; Robertson and Ustaomer, 2012; Robertson et al., 2004; Topuz et al., 2013).
7
8 More fundamentally, lithospheric modelling suggests that after slab breakoff, uplift will occur before
9
10 (and not after) surface magmatism (Davies and von Blanckenburg, 1995). Furthermore, isostatic
11
12 rebound following slab breakoff cannot explain the generation of multiple exposure and erosion
13
14 surfaces or why shallow-water conditions returned after each emergence event.
15
16
17

18
19 Instead, latest Jurassic-Early Cretaceous hiatuses around the Black Sea may be caused by rift-flank
20
21 uplift during rifting in the Greater Caucasus Basin (Vincent et al., 2016), western Black Sea (Derman,
22
23 2002; Nairn and Vincent, 2013) and possibly eastern Black Sea. The age of rifting in the Black Sea is
24
25 poorly constrained. Intriguingly, however, within the Greater Caucasus Basin subsidence analysis has
26
27 identified Late Tithonian to Berriasian and Hauterivian to Early Aptian rift events (Vincent et al.,
28
29 2016) that are within error of the hiatuses identified in this study (Figure 9). If regional extension
30
31 were the cause, then broad phases of rift-related subsidence and associated rift-flank uplift (rather
32
33 than near synchronous eustatically-generated events) should be expected. This, along with the
34
35 inherent imprecision of biostratigraphic determinations and the demonstrable removal of material
36
37 by erosion, would explain the apparent diachroneity of (i) the initial break-up of the Late Jurassic
38
39 Berdiga-Inalti-Yalta-Gerpigem carbonate platform around the Jurassic-Cretaceous boundary and (ii)
40
41 the subsequent recommencement and then interruption of Early Cretaceous sedimentation.
42
43
44
45
46
47

48
49 Secondary porosity development associated with the erosion surfaces identified in this study is not
50
51 extensive. This is possibly due to the relatively fine-grained nature of the inner platform carbonate
52
53 facies involved. Elsewhere around the Black Sea, however, secondary porosity development during
54
55 periods of subaerial exposure within higher energy outer platform grainstone, or platform edge or
56
57 isolated coral boundstone facies is far more pronounced (e.g. Figure 10). Our confirmation of the
58
59
60
61
62
63
64
65

1 likely regional extent of these subaerial exposure surfaces is therefore important for the reduction of
2 exploration risk offshore.
3

4
5 In conclusion, rift-flank uplift may be responsible for hiatus formation in the Kircaova section,
6 Eastern Pontides, although additional work is required to confirm a causal link. If this can be proven,
7 it would enhance our confidence that the disconformities and associated subaerial exposure /
8 karstification events identified in this study will also be developed within carbonate-dominated
9 sediments on the rift-generated Shatskiy Ridge and Mid Black Sea High. This might, in turn, result in
10 the development of intra-carbonate seismic markers and zones of porosity enhancement within this
11 potential reservoir interval in the Black Sea.
12
13
14
15
16
17
18
19
20
21
22
23
24
25

26 Acknowledgements

27
28
29 This paper is dedicated to the memory of the late A. Sami Derman without whom the fieldwork
30 associated with this research would not have been possible. We thank Anne Kelly for her Sr sample
31 preparation, Sarah Sherlock for her Ar-Ar analysis, Fiona Hyden for her siliciclastic petrographic
32 analysis, Marcin Krajewski for useful discussions and John McArthur for permission to use the
33 GTS2012 strontium sea level curve. We also acknowledge the insightful comments of Aral Okay,
34 Anton Kuznetsov and Giovanni Rusciadelli that helped improve the manuscript. The research was
35 funded by CASP's consortium of hydrocarbon exploration companies. RME acknowledges a Hugh
36 Kelly Research Fellowship from Rhodes University, South Africa. The paper is Cambridge Earth
37 Science contribution esc.4078.
38
39
40
41
42
43
44
45
46
47
48
49
50
51
52
53
54

55 References

56
57
58
59
60
61
62
63
64
65

1
2
3
4
5
6
7
8
9
10
11
12
13
14
15
16
17
18
19
20
21
22
23
24
25
26
27
28
29
30
31
32
33
34
35
36
37
38
39
40
41
42
43
44
45
46
47
48
49
50
51
52
53
54
55
56
57
58
59
60
61
62
63
64
65

Adamia, S.A., Akhvlediani, K.T., Kilasonia, V.M., Nairn, A.E.M., Papava, D., Patton, D.K., 1992. Geology of the Republic of Georgia: a review. *International Geology Review* 34, 447-476, doi: 10.1080/00206819209465614.

Afanasenkov, A.P., Nikishin, A.M., Obukhov, A.N., 2005. The system of Late Jurassic carbonate buildups in the northern Shatsky swell (Black Sea). *Doklady Earth Sciences* 403, 696-699.

Afanasenkov, A.P., Nikishin, A.M., Obukhov, A.N., 2007. Eastern Black Sea Basin: Geological Structure and Hydrocarbon Potential. Science World, Moscow (in Russian).

Altınar, D., Koçyiğit, A., Farinacci, A., Nicosia, U., Conti, M.A., 1991. Jurassic-Lower Cretaceous stratigraphy and paleogeographic evolution of the southern part of north-western Anatolia (Turkey). *Geologica Romana* 27, 13-80.

Aydın, M., Demir, O., Özçelik, Y., Terzioğlu, N., Satır, M., 1995. A geological revision of Inebolu, Devrekani, Ağlı and Küre areas; new observations in Paleotethys-Neotethys sedimentary successions, in: Erler, A., Ercan, T., Bingöl, E., Örcen, S. (Eds.), *Geology of the Black Sea Region, Proceedings of International Symposium on the Geology of the Black Sea Region*. Mineral Research and Exploration Institute (MTA), Ankara, Turkey, pp. 33-38.

BouDagher-Fadel, M.K., 2008. *Evolution and Geological Significance of Larger Benthic Foraminifera*. Elsevier, Amsterdam.

BouDagher-Fadel, M.K., 2012. *Biostratigraphic and Geological Significance of Planktonic Foraminifera*. Elsevier, Amsterdam.

BouDagher-Fadel, M.K., 2015. *Biostratigraphic and Geological Significance of Planktonic Foraminifera*, 2nd ed. OVPRL UCL, London.

Bucur, I.I., Granier, B., Krajewski, M., 2014. Calcareous algae, microbial structures and microproblematica from Upper Jurassic-lowermost Cretaceous limestones of southern Crimea. *Acta Palaeontologica Romaniae* 10, 61-86.

1
2
3
4
5
6
7
8
9
10
11
12
13
14
15
16
17
18
19
20
21
22
23
24
25
26
27
28
29
30
31
32
33
34
35
36
37
38
39
40
41
42
43
44
45
46
47
48
49
50
51
52
53
54
55
56
57
58
59
60
61
62
63
64
65

Burke, W.H., Denison, R.E., Hetherington, E.A., Koepnick, R.B., Nelson, H.F., Otto, J.B., 1982. Variation of seawater $^{87}\text{Sr}/^{86}\text{Sr}$ through Phanerozoic time. *Geology* 10, 516-519, doi: 10.1130/0091-7613(1982)10<516:VOSSTP>2.0.CO;2.

Chaykovskiy, B.P., Biletskiy, S.V., Deev, V.B., Demyan, O.S., Krasnorudska, S.I., 2006. Crimea Series sheets L-36-XXVIII (Evpatoriya) & L-36-XXXIV (Sevastopol'), in: Bilets'kiy, S.V. (Ed.), State Geological Map of Ukraine. Ministry of the Environment, State Geological Survey, Kiev, 1:200,000 (in Ukrainian).

Davies, H.J., von Blanckenburg, F., 1995. Slab breakoff: A model of lithosphere detachment and its test in the magmatism and deformation of collisional orogens. *Earth and Planetary Science Letters* 129, 85-102, doi: 10.1016/0012-821X(94)00237-S.

Denison, R.E., Koepeck, R.B., Fletcher, A., Howell, M.W., Calloway, W.S., 1994. Criteria for the retention of original seawater $^{87}\text{Sr}/^{86}\text{Sr}$ in ancient shelf limestones. *Chemical Geology: Isotope Geoscience section* 112, 131-143, doi: 10.1016/0009-2541(94)90110-4.

Derman, A.S., 2002. Black Sea rift sequences. *Türkiye Petrol Jeologları Derneği Bülteni* 14, 36-65.

Derman, A.S., İztan, Y.H., 1997. Results of geochemical analysis of seeps and potential source rocks from Northern Turkey and the Turkish Black Sea, in: Robinson, A.G. (Ed.), *Regional and Petroleum Geology of the Black Sea and Surrounding Region*. AAPG Memoir, vol. 68, Tulsa, Oklahoma, pp. 313-330, doi: 10.1306/M68612C16.

Derman, A.S., Sayılı, A., 1995. İnalti Formation; a key unit for regional geology, in: Erler, A., Ercan, T., Bingöl, E., Örcen, S. (Eds.), *Geology of the Black Sea Region, Proceeding of International Symposium on the Geology of the Black Sea Region*. Mineral Research and Exploration Institute (MTA), Ankara, Turkey, pp. 104-108.

Dokuz, A., Aydınçakır, E., Kandemir, R., Karslı, O., Siebel, W., Derman, A.S., Turan, M., 2017. Late Jurassic magmatism and stratigraphy in the Eastern Sakarya Zone, Turkey: Evidence for the slab breakoff of Paleotethyan oceanic lithosphere. *Journal of Geology* 125, 1-31, doi: 10.1086/689552.

1 Dokuz, A., Karsli, O., Chen, B., Uysal, I., 2010. Sources and petrogenesis of Jurassic granitoids in the
2 Yusufeli area, Northeastern Turkey: Implications for pre- and post-collisional lithospheric thinning of
3 the eastern Pontides. *Tectonophysics* 480, 259-279, doi: 10.1016/j.tecto.2009.10.009.
4

5
6 Dokuz, A., Tanyolu, E., 2006. Geochemical constraints on the provenance, mineral sorting and
7 subaerial weathering of Lower Jurassic and Upper Cretaceous clastic rocks of the Eastern Pontides,
8 Yusufeli (Artvin), NE Turkey. *Turkish Journal of Earth Sciences* 15, 181-209.
9

10
11 Elderfield, H., 1986. Strontium isotope stratigraphy. *Palaeogeography Palaeoclimatology*
12 *Palaeoecology* 57, 71-90, doi: 10.1016/0031-0182(86)90007-6.
13

14
15 Eren, M., 1983. Gümüşhane-Kale Arasının Jeolojisi ve Mikrofasiyes İncelemesi. MSc thesis, Karadeniz
16 Technical University, Trabzon, Turkey (in Turkish).
17

18
19 Eren, M., Tasli, K., 2002. Kilop Cretaceous hardground (Kale, Gümüşhane, NE Turkey): description
20 and origin. *Journal of Asian Earth Sciences* 20, 433-448, doi: 10.1016/S1367-9120(01)00027-X.
21

22
23 Fikolina, L.A., Bilokric, O.O., Obshars'ka, N.O., Krasnoruds'ka, S.I., Udovychenko, N.I., 2008. Crimea
24 Series sheets L-36-XXIX (Simferopol) & L-36-XXXV (Yalta), in: Semenenko, V.N. (Ed.), State Geological
25 Map Ukraine. Ministry of the Environment, State Geological Survey, Kiev, 1:200,000 (in Ukrainian).
26

27
28 Golonka, J., 2004. Plate tectonic evolution of the southern margin of Eurasia in the Mesozoic and
29 Cenozoic. *Tectonophysics* 381, 235-273, doi: 10.1016/j.tecto.2002.06.004.
30

31
32 Gorokhov, I.M., Semikhatov, M.A., Baskakov, A.V., Kutuyavin, E.P., Mel'nikov, N.N., Sochava, A.V.,
33 Turchenko, T.L., 1995. Sr isotopic composition in Riphean, Vendian, and Lower Cambrian carbonates
34 from Siberia. *Stratigraphy and Geological Correlation* 3, 1-28.
35

36
37 Görür, N., 1988. Timing of opening of the Black Sea basin. *Tectonophysics* 147, 247-262, doi:
38 10.1016/0040-1951(88)90189-8.
39

40
41 Görür, N., Şengör, A.M.C., Akkök, R., Yılmaz, Y., 1983. Pontidlerde Neo-Tetis'in kuzey kolunun
42 açılmasına ilişkin sedimentolojik veriler (Sedimentological data regarding the opening of the
43 northern branch of Neotethys in the Pontides). *Türkiye Jeoloji Kurumu Bülteni* 26, 11-19 (in Turkish).
44
45
46
47
48
49
50
51
52
53
54
55
56
57
58
59
60
61
62
63
64
65

1 Gradstein, F.M., Ogg, J.G., Schmitz, M.D., Ogg, G.M., 2012. A Geologic Time Scale 2012. Elsevier,
2 Oxford, p. 1144.
3

4 Guo, L., Vincent, S.J., Lavrishchev, V.A., 2011. Upper Jurassic reefs from the Russian western
5 Caucasus: implications for the Eastern Black Sea. Turkish Journal of Earth Sciences 20, 629-653, doi:
6 10.3906/yer-1012-5.
7

8 Haq, B.U., 2014. Cretaceous eustasy revisited. Global and Planetary Change 113, 44-58, doi:
9 10.1016/j.gloplacha.2013.12.007.
10

11 Kandemir, R., 2004. Sedimentary characteristics and depositional conditions of Lower-Middle
12 Jurassic Şenköy Formation in and around Gümüşhane. PhD thesis, Karadeniz Technical University,
13 Trabzon, Turkey (in Turkish).
14

15 Kandemir, R., Yılmaz, C., 2009. Lithostratigraphy, facies, and depositional environment of the Lower
16 Jurassic Ammonitico Rosso type sediments (ARTS) in the Gümüşhane area, NE Turkey: implications
17 for the opening of the northern branch of the Neo-Tethys Ocean. Journal of Asian Earth Sciences 34,
18 586-598, doi: 10.1016/j.jseaes.2008.08.006.
19

20 Kara-Gülbay, R., Ziya Kırmacı, M., Korkmaz, S., 2012. Organic geochemistry and depositional
21 environment of the Aptian bituminous limestone in the Kale Gümüşhane area (NE-Turkey): An
22 example of lacustrine deposits on the platform carbonate sequence. Organic Geochemistry 49, 6-17,
23 doi: 10.1016/j.orggeochem.2012.05.006.
24

25 Karsli, O., Dokuz, A., Uysal, I., Aydin, F., Kandemir, R., Wijbrans, J., 2010. Generation of the Early
26 Cenozoic adakitic volcanism by partial melting of mafic lower crust, Eastern Turkey: Implications for
27 crustal thickening to delamination. Lithos 114, 109-120, doi: 10.1016/j.lithos.2009.08.003.
28

29 Kaya, M., Altiner, D., 2015. Microencrusters from the Upper Jurassic–Lower Cretaceous İnaltı
30 Formation (Central Pontides, Turkey): remarks on the development of reefal/peri-reefal facies.
31 Facies 61, 1-25, doi: 10.1007/s10347-015-0445-5.
32

33 Kaz'min, V.G., Tikhonova, N.F., 2006. Evolution of Early Mesozoic back-arc basins in the Black Sea-
34 Caucasus segment of a Tethyan active margin, in: Robertson, A.H.F., Mountrakis, D. (Eds.), Tectonic
35

36
37
38
39
40
41
42
43
44
45
46
47
48
49
50
51
52
53
54
55
56
57
58
59
60
61
62
63
64
65

1 Development of the Eastern Mediterranean Region. Geological Society Special Publications, London,
2 vol. 260, pp. 179-200, doi: 10.1144/GSL.SP.2006.260.01.08.
3

4 Kazmin, V.G., 2006. Tectonic evolution of the Caucasus and Fore-Caucasus in the Late Paleozoic.
5 Doklady Earth Sciences 406, 1-3.
6

7 Kazmin, V.G., Sbortshikov, I.M., Ricou, L.-E., Zonenshain, L.P., Boulin, J., Knipper, A.L., 1986. Volcanic
8 belts as markers of the Mesozoic-Cenozoic active margin of Eurasia. Tectonophysics 123, 123-152,
9 doi: 10.1016/0040-1951(86)90195-2.
10

11 Kazmin, V.G., Schreider, A.A., Bulychev, A.A., 2000. Early stages of evolution of the Black Sea, in:
12 Bozkurt, E., Winchester, J.A., Piper, J.D.A. (Eds.), Tectonics and Magmatism in Turkey and the
13 Surrounding Area. Geological Society, London, Special Publication, vol. 173, pp. 235-249, doi:
14 10.1144/GSL.SP.2000.173.01.12.
15

16 Ketin, İ., Gümüş, O., 1963. Sinop-Ayancık güneyinde üçüncü bölgeye dahil sahaların jeolojisi
17 hakkında rapor - kısım Jura ve Kretase formasyonlarının etüdü. TPAO Arşivi rap no. 288, Ankara (in
18 Turkish).
19

20 Kiessling, W., Flügel, E., Golonka, J., 1999. Paleoreef maps: evaluation of a comprehensive database
21 on Phanerozoic reefs. American Association of Petroleum Geologist Bulletin 83, 1552-1587.
22

23 Kırmacı, M.Z., 1992. Alucra-Gümüşhane-Bayburt Yörelerindeki (Dogu Pontid Güney Zonu) Üst Jura-
24 Alt Kretase Yaslı Berdiga Kireçtası' nın Sedimentolojik incelemesi, Fen Bilimleri Enstitüsü. PhD thesis,
25 Karadeniz Teknik Üniversitesi, Trabzon (in Turkish).
26

27 Kırmacı, M.Z., Koch, R., Buccur, I.I., 1996. An Early Cretaceous Section in the Kirchaova Area (Berdiga
28 Limestone, NE - Turkey) and its correlation with Platform Carbonates in W-Slovenia. Facies 34, 1-22,
29 doi: 10.1007/BF02546154.
30

31 Koch, R., Bucur, I.I., Kırmacı, M.Z., Eren, M., Tasli, K., 2008. Upper Jurassic and Lower Cretaceous
32 carbonate rocks of the Berdiga Limestone – Sedimentation on an onbound platform with volcanic
33 and episodic siliciclastic influx. Biostratigraphy, facies and diagenesis (Kircaova, Kale-Gümüşhane
34
35
36
37
38
39
40
41
42
43
44
45
46
47
48
49
50
51
52
53
54
55
56
57
58
59
60
61
62
63
64
65

1
2 area; NE-Turkey). Neues Jahrbuch für Geologie und Paläontologie, Abhandlungen 247, 23-61, doi:
3 10.1127/0077-7749/2008/0247-0023.

4 Koçyiğit, A., Altıner, D., 2002. Tectonostratigraphic evolution of the North Anatolian palaeorift
5 (NAPR): Hettangian-Aptian passive continental margin of the northern Neo-Tethys, Turkey. Turkish
6 Journal of Earth Sciences 11, 169-191.

7
8
9
10
11 Konak, N., Okay, A.I., Hakyemez, H.Y., 2009. Tectonics and Stratigraphy of the Eastern Pontides, 2nd
12 International Symposium on the Geology of the Black Sea Region. General Directorate of Mineral
13 Research and Exploration (MTA) / TMMOB, Ankara, Turkey.

14
15
16
17
18
19
20
21
22
23
24
25
26
27
28
29
30
31
32
33
34
35
36
37
38
39
40
41
42
43
44
45
46
47
48
49
50
51
52
53
54
55
56
57
58
59
60
61
62
63
64
65

Korsakov, S.G., Semenukha, I.N., Beluzhenko, E.V., Chernykh, V.I., Tuzikov, G.R., Grekov, I.I., Tokarev,
V.N., Derkachëva, M.G., Sokolov, V.V., 2004. National Geological Map of the Russian Federation,
Caucasus series sheet L-37-XXXV (Maykop), 2nd edition ed. St. Petersburg cartographic enterprise of
VSEGEI, Moscow, 1:200,000 (in Russian).

Korsakov, S.G., Semenukha, V.M., Andreev, N.M., 2002. National Geological Map of the Russian
Federation, Caucasus series sheet L-37-XXXIV (Tuapse), 2nd edition ed. St. Petersburg cartographic
enterprise of VSEGEI, Moscow, 1:200,000 (in Russian).

Kuznetsov, A.B., Semikhatov, M.A., Gorokhov, I.M., 2012. The Sr isotope composition of the world
ocean, marginal and inland seas: Implications for the Sr isotope stratigraphy. Stratigraphy and
Geological Correlation 20, 501-515, doi: 10.1134/s0869593812060044.

Leinfelder, R., Schmid, D.U., Nose, M., Werner, W., 2002. Jurassic reef patterns - the expression of a
changing globe, in: Kiessling, W., Flügel, E., Golonka, J. (Eds.), Phanerozoic Reef Patterns. SEPM,
Special Publication, vol. 72, Tulsa, OK, pp. 465-520.

Masse, J.-P., Tüysüz, O., Fenerci-Masse, M., Özer, S., Sari, B., 2009. Stratigraphic organisation, spatial
distribution, palaeoenvironmental reconstruction, and demise of Lower Cretaceous (Barremian-
lower Aptian) carbonate platforms of the Western Pontides (Black Sea region, Turkey). Cretaceous
Research 30, 1170-1180, doi: 10.1016/j.cretres.2009.05.004.

1
2
3
4
5
6
7
8
9
10
11
12
13
14
15
16
17
18
19
20
21
22
23
24
25
26
27
28
29
30
31
32
33
34
35
36
37
38
39
40
41
42
43
44
45
46
47
48
49
50
51
52
53
54
55
56
57
58
59
60
61
62
63
64
65

McArthur, J.M., Howarth, R.J., Bailey, T.R., 2001. Strontium Isotope Stratigraphy: LOWESS version 3: best fit to the marine Sr-isotope curve for 0-509 Ma and accompanying look-up table for deriving numerical age. *The Journal of Geology* 109, 155-170, doi: 10.1016/j.cretres.2009.05.004.

McArthur, J.M., Howarth, R.J., Shields, G.A., 2012. Strontium Isotope Stratigraphy, in: Gradstein, F.M., Ogg, J.G., Schmitz, M.D., Ogg, G.M. (Eds.), *A Geologic Time Scale 2012*. Elsevier, Oxford, pp. 127-144.

Meisner, A., Krylov, O., Nemcok, M., 2009. Development and structural architecture of the Eastern Black Sea. *The Leading Edge* 28, 1046-1055, doi: 10.1190/1.3236374.

Nairn, S., Vincent, S.J., 2013. A review of the Cretaceous-Eocene geology of the Turkish margin of the Black Sea. *CASP Black Sea Project report 38*, Cambridge.

Nikishin, A.M., Okay, A., Tüysüz, O., Demirer, A., Wannier, M., Amelin, N., Petrov, E., 2015a. The Black Sea basins structure and history: new model based on new deep penetration regional seismic data. Part 2: Tectonic history and paleogeography. *Marine and Petroleum Geology* 59, 656-670, doi: 10.1016/j.marpetgeo.2014.08.017.

Nikishin, A.M., Okay, A.I., Tüysüz, O., Demirer, A., Amelin, N., Petrov, E., 2015b. The Black Sea basins structure and history: new model based on new deep penetration regional seismic data. Part 1: Basins structure and fill. *Marine and Petroleum Geology* 59, 638-655, doi: 10.1016/j.marpetgeo.2014.08.018.

Nikishin, A.M., Wannier, M., Alekseev, A.S., Almendinger, O.A., Fokin, P.A., Gabdullin, R.R., Khudoley, A.K., Kopaevich, L.F., Mityukov, A.V., Petrov, E.I., Rubtsova, E.V., 2015c. Mesozoic to recent geological history of southern Crimea and the Eastern Black Sea region, in: Sosson, M., Stephenson, R.A., Adamia, S.A. (Eds.), *Tectonic Evolution of the Eastern Black Sea and Caucasus*. Geological Society, Special Publications, London, vol. 428, pp. 241-264, doi: 10.1144/SP428.1.

Okay, A.I., 1996. Granulite Facies Gneisses from the Pular Region, Eastern Pontides. *Turkish Journal of Earth Sciences* 5, 55-61.

1 Okay, A.I., 2000. Was the Late Triassic orogeny in Turkey caused by the collision of an oceanic
2 plateau?, in: Bozkurt, E., Winchester, J.A., Piper, J.D.A. (Eds.), *Tectonics and Magmatism in Turkey*
3 *and the Surrounding Area*. Geological Society, London, Special Publication, vol. 173, pp. 25-41, doi:
4 10.1144/GSL.SP.2000.173.01.02.
5
6

7
8
9 Okay, A.I., Altiner, D., Sunal, G., Aygül, M., Akdoğan, R., Altiner, S., Simmons, M., 2017. Geological
10 evolution of the Central Pontides, in: Simmons, M.D., Tari, G.C., Okay, A.I. (Eds.), *Petroleum Geology*
11 *of the Black Sea*. Geological Society Special Publications, London, vol. 464, doi: 10.1144/SP464.3.
12
13

14
15
16 Okay, A.I., Leven, E.J., 1996. Stratigraphy and paleontology of the Upper Palaeozoic sequences in the
17 Pulur (Bayburt) region, Eastern Pontides. *Turkish Journal of Earth Sciences* 5, 145-155.
18
19

20
21 Okay, A.I., Nikishin, A.M., 2015. Tectonic evolution of the southern margin of Laurasia in the Black
22 Sea region. *International Geology Review* 57, 1051-1076, doi: 10.1080/00206814.2015.1010609.
23
24

25
26 Okay, A.I., Şahintürk, O., 1997. Geology of the Eastern Pontides, in: Robinson, A.G. (Ed.), *Regional*
27 *and Petroleum Geology of the Black Sea and Surrounding Region*. AAPG Memoir, vol. 68, Tulsa,
28 Oklahoma, pp. 291-311, doi: 10.1306/M68612C15.
29
30

31
32
33 Okay, A.I., Sunal, G., Sherlock, S., Altiner, D., Tüysüz, O., Kylander-Clark, A.R.C., Aygül, M., 2013. Early
34 Cretaceous sedimentation and orogeny on the active margin of Eurasia: Southern Central Pontides,
35 Turkey. *Tectonics* 32, 1247-1271, doi: 10.1002/tect.20077.
36
37
38

39
40 Okay, A.I., Sunal, G., Tuysuz, O., Sherlock, S., Keskin, M., Kylander-Clark, A.R.C., 2014. Low-pressure-
41 high-temperature metamorphism during extension in a Jurassic magmatic arc, Central Pontides,
42 Turkey. *Journal of Metamorphic Geology* 32, 49-69, doi: 10.1111/jmg.12058.
43
44
45

46
47 Okay, A.I., Topuz, G., 2017. Variscan orogeny in the Black Sea region. *International Journal of Earth*
48 *Sciences* 106, 569-592, doi: 10.1007/s00531-016-1395-z.
49
50

51
52 Okay, A.I., Tüysüz, O., 1999. Tethyan sutures of northern Turkey, in: Durand, B., Jolivet, L., Horváth,
53 F., Séranne, M. (Eds.), *The Mediterranean Basins: Tertiary Extension within the Alpine Orogen*.
54 Geological Society, London, Special Publication, vol. 156, pp. 475-515, doi:
55 10.1144/GSL.SP.1999.156.01.22.
56
57
58
59
60
61
62
63
64
65

1
2
3
4
5
6
7
8
9
10
11
12
13
14
15
16
17
18
19
20
21
22
23
24
25
26
27
28
29
30
31
32
33
34
35
36
37
38
39
40
41
42
43
44
45
46
47
48
49
50
51
52
53
54
55
56
57
58
59
60
61
62
63
64
65

Pelin, S., 1977. Alucra (Giresun) Güneydoğu Yöresinin Petrol Olanakları Bakımından Jeolojik İncelemesi. PhD thesis, Karadeniz Technical University, Trabzon, Turkey (in Turkish).

Pickett, E.A., Robertson, A.H.F., 2004. Significance of the volcanogenic Nilüfer Unit and related components of the Triassic Karakaya Complex for Tethyan subduction/accretion processes in NW Turkey. *Turkish Journal of Earth Sciences* 13, 97-143.

Robertson, A., Parlak, O., Ustaomer, T., Tasli, K., Inan, N., Dumitrica, P., Karaoglan, F., 2014. Subduction, ophiolite genesis and collision history of Tethys adjacent to the Eurasian continental margin: new evidence from the Eastern Pontides, Turkey. *Geodinamica Acta* 26, 230-293, doi: 10.1080/09853111.2013.877240.

Robertson, A.H.F., Dixon, J.E., 1984. Introduction: aspects of the geological evolution of the Eastern Mediterranean, in: Dixon, J.E., Robertson, A.H.F. (Eds.), *The geological evolution of the Eastern Mediterranean*. Geological Society Special Publication, London, vol. 17, pp. 1-74, doi: 10.1144/GSL.SP.1984.017.01.02.

Robertson, A.H.F., Ustaomer, T., 2012. Testing alternative tectono-stratigraphic interpretations of the Late Palaeozoic-Early Mesozoic Karakaya Complex in NW Turkey: Support for an accretionary origin related to northward subduction of Palaeotethys. *Turkish Journal of Earth Sciences* 21, 961-1007, doi: 10.3906/yer-1003-22.

Robertson, A.H.F., Ustaömer, T., Pickett, E.A., Collins, A.S., Andrew, T., Dixon, J.E., 2004. Testing models of Late Palaeozoic-Early Mesozoic orogeny in Western Turkey: support for an evolving open-Tethys model. *Journal of the Geological Society, London* 161, 501-511, doi: 10.1144/0016-764903-080.

Robinson, A.G., Banks, C.J., Rutherford, M.M., Hirst, J.P.P., 1995. Stratigraphic and structural development of the Eastern Pontides, Turkey. *Journal of the Geological Society, London* 152, 861-872, doi: 10.1144/gsjgs.152.5.0861.

1 Rud'ko, S.V., Kuznetsov, A.B., Piskunov, V.K., 2014. Sr isotope chemostratigraphy of the Upper
2 Jurassic carbonate rocks in the Demerdzhi Plateau (Crimean Mountains). *Stratigraphy and Geological*
3
4 *Correlation* 22, 494-506.
5

6 Rud'ko, S.V., Kuznetsov, A.B., Pokrovsky, B.G., 2017. Sr chemostratigraphy, $\delta^{13}\text{C}$, and $\delta^{18}\text{O}$ of rocks in
7 the Crimean carbonate platform (Late Jurassic, Northern Peri-Tethys). *Lithology and Mineral*
8
9 *Resources* 52, 479-497.
10

11 Şengör, A.M.C., Yılmaz, Y., 1981. Tethyan evolution of Turkey: a plate tectonic approach.
12
13 *Tectonophysics* 75, 181-241, doi: 10.1016/0040-1951(81)90275-4.
14

15 Taslı, K., 1997. Stratigraphical and paleontological data on the Malm volcanism in the eastern
16
17 Pontides (NE Turkey). *Istanbul University Earth Sciences Bulletin* 8, 95-101 (in Turkish).
18

19 Taslı, K., Özer, E., Yılmaz, C., 1999. Biostratigraphic and environmental analysis of the Upper Jurassic-
20
21 Lower Cretaceous carbonate sequence in the Basoba Yayla area (Trabzon, NE Turkey). *Turkish*
22
23 *Journal of Earth Sciences* 8, 125-135.
24

25 Taslı, K., Özsayar, T., 1997. Stratigraphy and paleoenvironmental setting of the Albian-Campanian
26
27 carbonate sequence in the Gümüşhane province (Eastern Pontides, NE Turkey). *TAPG Bulletin* 9, 13-
28
29 29 (in Turkish).
30

31 Tokel, S., 1972. Stratigraphical and volcanic history of the Gümüşhane region, NE Turkey. PhD thesis,
32
33 University College London, UK.
34

35 Topuz, G., Altherr, R., Kalt, A., Satır, M., Werner, O., Schwarz, W.H., 2004a. Aluminous granulites
36
37 from the Pulur complex, NE Turkey: a case of partial melting, efficient melt extraction and
38
39 crystallisation. *Lithos* 72, 183-207, doi: 10.1007/s00531-003-0372-5.
40

41 Topuz, G., Altherr, R., Satır, M., Schwarz, W., 2004b. Low-grade metamorphic rocks from the Pulur
42
43 complex, NE Turkey: implications for the pre-Liassic evolution of the Eastern Pontides. *International*
44
45 *Journal of Earth Sciences* 93, 72-91, doi: 10.1016/j.lithos.2003.10.002.
46
47
48
49
50
51
52
53
54
55
56
57
58
59
60
61
62
63
64
65

1 Topuz, G., Altherr, R., Schwarz, W., Dokuz, A., Meyer, H.-P., 2007. Variscan amphibolite-facies rocks
2 from the Kurtoğlu metamorphic complex (Gümüşhane area, Eastern Pontides, Turkey). *International*
3 *Journal of Earth Sciences* 96, 861-873, doi: 10.1007/s00531-006-0138-y.
4
5
6 Topuz, G., Altherr, R., Siebel, W., Schwarz, W.H., Zack, T., Hasözbeğ, A., Barth, M., Satır, M., Sen, C.,
7
8
9 2010. Carboniferous high-potassium I-type granitoid magmatism in the Eastern Pontides: The
10 Gümüşhane pluton (NE Turkey). *Lithos* 116, 92-110, doi: 10.1016/j.lithos.2010.01.003.
11
12 Topuz, G., Göçmengil, G., Rolland, Y., Çelik, Ö.F., Zack, T., Schmitt, A.K., 2013. Jurassic accretionary
13
14 complex and ophiolite from northeast Turkey: No evidence for the Cimmerian continental ribbon.
15
16
17
18
19 *Geology* 41, 255-258, doi: 10.1130/g33577.1.
20
21 Tüysüz, O., 1990. Tectonic evolution of a part of the Tethyside orogenic collage: the Kargı Massif,
22
23
24 northern Turkey. *Tectonics* 9, 141-160, doi: 10.1029/TC009i001p00141.
25
26 Ustaömer, T., Robertson, A.H.F., 2010. Late Palaeozoic-Early Cenozoic tectonic development of the
27
28 Eastern Pontides (Artvin area), Turkey: stages of closure of Tethys along the southern margin of
29
30 Eurasia, in: Sosson, M., Kaymakci, N., Stephenson, R.A., Bergerat, F., Starostenko, V. (Eds.),
31
32
33 Sedimentary basin tectonics from the Black Sea and Caucasus to the Arabian Platform. *Geological*
34
35
36 Society, London, Special Publication, vol. 340, pp. 281-327, doi: 10.1144/SP340.13.
37
38 Vincent, S.J., Braham, W., Lavrishchev, V.A., Maynard, J.R., Harland, M., 2016. The formation and
39
40 inversion of the western Greater Caucasus Basin and the uplift of the western Greater Caucasus:
41
42
43 Implications for the wider Black Sea region. *Tectonics* 35, 2948-2962, doi: 10.1002/2016TC004204.
44
45 Yılmaz, C., 1992. Kelkit (Gümüşhane) Yöresinin Stratigrafisi. *Jeoloji Mühendisliği Dergisi* 40, 50-62 (in
46
47
48 Turkish).
49
50 Yılmaz, C., 2002. Tectono-sedimentary records and controlling factors of the Mesozoic sedimentary
51
52 basin in the Gümüşhane-Bayburt region. *Türkiye Jeoloji Bülteni* 45, 141-164 (in Turkish).
53
54 Yılmaz, C., Kandemir, R., 2006. Sedimentary records of the extensional tectonic regime with
55
56
57 temporal cessation: Gümüşhane Mesozoic Basin (NE Turkey). *Geologica Carpathica* 57, 3-13.
58
59
60
61
62
63
64
65

1
2
3
4
5
6
7
8
9
10
11
12
13
14
15
16
17
18
19
20
21
22
23
24
25
26
27
28
29
30
31
32
33
34
35
36
37
38
39
40
41
42
43
44
45
46
47
48
49
50
51
52
53
54
55
56
57
58
59
60
61
62
63
64
65

Yılmaz, Y., Tüysüz, O., Yiğitbaş, E., Can Genç, S., Şengör, A.M.C., 1997. Geology and tectonic evolution of the Pontides, in: Robinson, A.G. (Ed.), Regional and Petroleum Geology of the Black Sea and Surrounding Region. AAPG Memoir, vol. 68, Tulsa, Oklahoma, pp. 183-226, doi: 10.1306/M68612C11.

Table captions

Table 1. Summary of the stratigraphic units identified in the Middle or Upper Jurassic to Lower Cretaceous Kircaova section in the Eastern Pontides (locality PT09_21E).

Table 2. Micropaleontological analyses of selected thin sections from locality PT09_21 in the Eastern Pontides. Ages are based on first appearance Planktonic Foraminiferal zones, Shallow Benthic zones and letter stages after BouDagher-Fadel (2008, 2012, 2015). See Figure 2 and Figure 4 for their location.

Table 3. Sample ages derived from the Sr isotope seawater curve (McArthur et al., 2012), using foraminiferal data from the same section and stratigraphic position to discriminate between multiple possible positions on the curve. Minimum and maximum age uncertainty is calculated to include both the analytical error (2σ) and the uncertainty on the seawater curve. Note that the stratigraphic height relative to the base of section does not always correspond to stratigraphic position because of the relief on the erosion surface. See Figure 2 and Figure 4 for their location.

Table 4. Micropaleontological analyses of selected thin sections from the section south of Küre at locality PT09_017 (41.70450°N, 33.69394°E) in the Central Pontides. Ages are based on first appearance Planktonic Foraminiferal zones, Shallow Benthic zones and letter stages after BouDagher-Fadel (2008, 2012, 2015).

Figure captions

1
2
3 Figure 1. Tectonic map of the Black Sea region showing eastern Sakarya and the Kircaova section in
4 its regional context. Modified from Okay and Tüysüz (1999). Abbreviations: AM = Ağvanis Massif; PM
5 = Pulur Massif; ATB = Adjara-Trialet Belt.
6
7

8
9
10 Figure 2. Panorama of Upper Jurassic – Lower Cretaceous strata at Kircaova (locality PT09_21E) with
11 sample positions, the stratigraphic subdivisions of Koch et al. (2008) and the four erosion surfaces
12 (A-D) and lava flow marked. The field of view is located on Figure 3.
13
14
15

16
17
18 Figure 3. Geological map showing the outcrop pattern of the Berdiga Formation to the south of Kale
19 in the Gümüşhane region of the Eastern Pontides. The main logged section at locality PT09_21E is
20 known as the Kircaova section after the previous work of Koch et al. (2008). Additional information
21 and samples were collected from the lower part of the formation at locality PT09_21B. These were
22 correlated using the lava flow at 70 m in the logged section (Figure 4). The base of the section was
23 also observed at locality PT09_21A. Modified from Kandemir (2004) and Karsli et al. (2010).
24
25
26

27
28
29 Figure 4. Summary stratigraphy of locality PT09_21 in the Eastern Pontides showing the main facies,
30 the key erosional / subaerially exposed surfaces and the strontium and *in situ* foraminiferal age
31 ranges. The strontium age uncertainties include both the analytical error (2σ) and the uncertainty on
32 the seawater curve (see Figure 8). The maximum and minimum permitted age ranges of the hiatuses
33 (light and dark grey shading, respectively) are based on the age uncertainties of the samples that
34 bracket the hiatuses. Note that the Sr-derived ages are much more precise than those provided by
35 the foraminiferal ages alone. Samples are located on Figure 2. The stage boundaries are from
36 Gradstein et al. (2012).
37
38
39
40
41
42
43
44
45
46
47
48
49
50
51

52
53
54 Figure 5. Typical carbonate facies in thin section from Upper Jurassic – Lower Cretaceous strata at
55 Kircaova (locality PT09_21E) in the eastern Pontides. A) Large bivalve shells within a gastropod
56 floatstone. Note the occurrence of pendant cement lining an early dissolved bivalve shell (black
57
58
59
60
61
62
63
64
65

1 arrow) that is indicative of meteoric dissolution and cementation in a vadose environment. Also note
2 the micritic envelopes (white arrow) and blocky spar calcite cement (b). Sample 21E_02. B) Lime
3 mudstone; note the ostracod (black arrow) and rare dolomite crystals (white arrow). Sample
4 21B_03. C) Dolostone whose original texture is completely altered by fine-grained dolomite with
5 scattered dissolution vugs. Sample 21E_14. D) Intraclastic-bioclastic grainstone facies comprising
6 intraclasts (bioclastic limestones) and abundant small benthic foraminifera and bivalves. Note the
7 pore spaces filled with isopachous (black arrow) and drusy (d) calcite cements. Sample 21E_17.
8 E) Foraminifera packstone-grainstone facies with abundant small (miliolids) and large benthic
9 foraminifera in a partly grain- and partly mud-supported matrix. Sample 21E_23. Unlike other
10 samples in units X-XII, this sample has not been affected by dolomitisation. F) Limestone clasts from
11 the erosion surface C are cemented by clays in a meniscus style (black arrow), which was formed in a
12 vadose environment. Sample 21E_28.

13
14
15
16
17
18
19
20
21
22
23
24
25
26
27
28
29 Figure 6. Field photographs of the erosion surfaces A-D within Upper Jurassic – Lower Cretaceous
30 strata at Kircaova (locality PT09_21E). A) Relief on erosion surface A on the northwestern margin of
31 its incised valley. B) Approximately 45 m of relief on erosion surface A on the southeastern margin of
32 its incised valley. C) Brecciated limestones at the top of unit V at erosion surface A. D) Erosion
33 surface B overlain by sandstones, laminated limestones and limestone breccias. E) Detail of the
34 micrite-cemented limestone breccia above erosion surface B. F) Erosion surface C overlain by
35 limestone conglomerates with clasts up to 10 cm in diameter. G) Erosion surface D overlain by
36 poorly cemented limestone breccias, which include reworked calcrete peds, and laminated
37 limestones. See Figure 2 and Figure 4 for the wider context of these erosion surfaces.

38
39
40
41
42
43
44
45
46
47
48
49
50
51 Figure 7. Selected foraminiferal photomicrographs of samples from locality PT09_21. 1) *A-Debarina*
52 *hahounerensis* Forcade, Raoult and Vila, B-*Vercorsella arenata* Arnaud-Vanneau, Sample 21E_33,
53 x30. 2) *Pseudolituonella gavonensis* Foury, Sample 21E_33, x20. 3) *Debarina hahounerensis* Forcade
54 Sample 21E_33, x15. 4-5) *Vercorsella arenata* Arnaud-Vanneau, 4, Sample 21E_33; 5, Sample
55
56
57
58
59
60
61
62
63
64
65

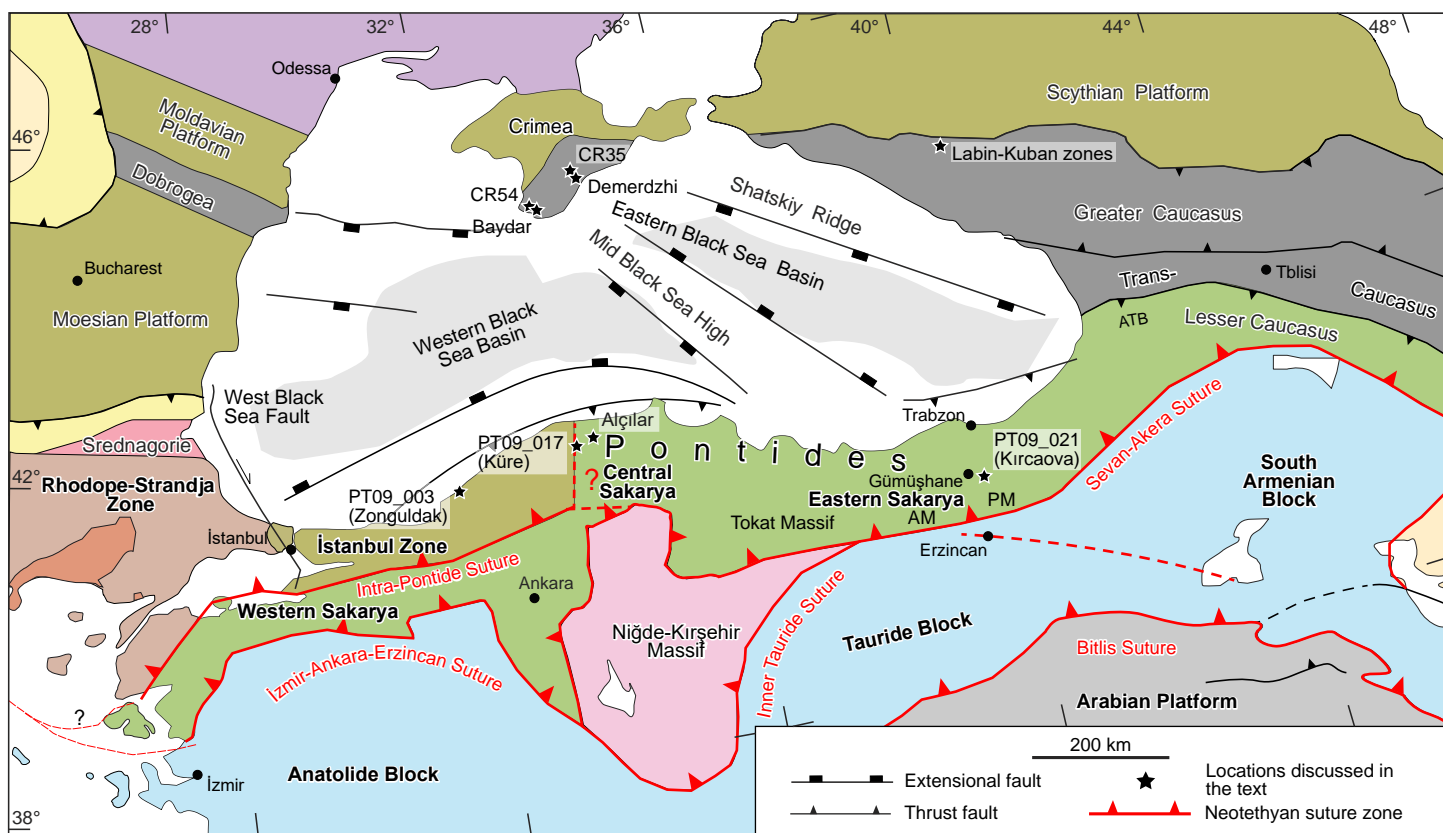
1 S_PT09_SV_21E_27, x30. 6) *Praechrysalidina infracretacea* Luperto Sinni, Sample 21E_27, x18.
2
3 7) *Andersenolina elongata* (Leupold), Sample 21E_16, x56. 8) *A-Cuneolina camposaurii* Sartoni and
4 Crescenti. B-*Andersenolina elongata* (Leupold), Sample 21E_17, x20. 9) *A-Andersenolina elongata*
5 (Leupold). B-*Praechrysalidina infracretacea* Luperto Sinni, Sample 21E_16, x28. 10-
6
7 11) *Pseudocyclammina lituus* (Yokoyama) Sample 21E_02, 10, x28; 11, x32. 12) *Rectocyclammina*
8
9 *chouberti* Hottinger, Sample 21E_02, x22. 13-14) *Alveosepta jaccardi* (Schrodt), Sample 21E_02, 13,
10
11 x45; 14, x58. 15) *Pseudocyclammina* sp., Sample 21E_02, 13, x20. 16) *Mesoendothyra* sp., Sample
12
13 21E_02, x60. 17) *Trocholina conica* (Schlumberger), Sample 21B_08, x80.
14
15
16
17
18
19

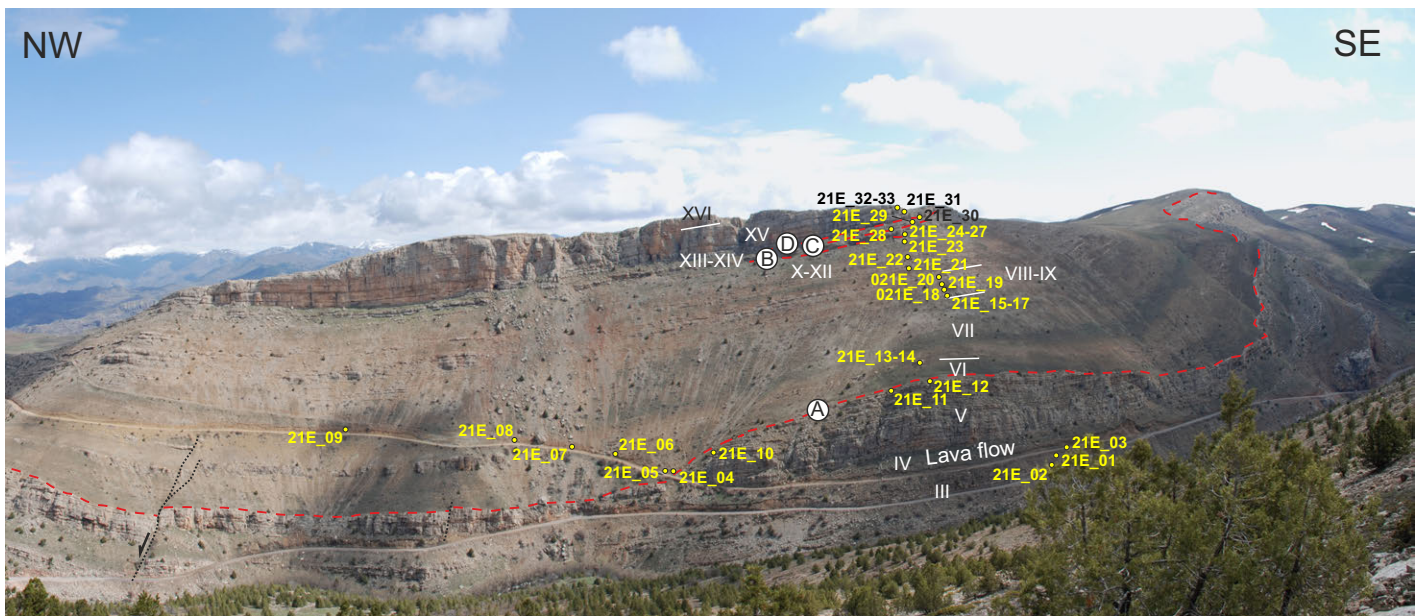
20 Figure 8. Measured Sr isotope ratio and analytical error (2σ) of the samples in this study plotted
21 against best age estimate and its uncertainty as derived from the Sr isotope seawater curve
22 (McArthur et al., 2012). Insert illustrates that multiple ages can be interpreted from the Sr isotope
23 seawater curve between 100-200 Ma. The most likely ages have been identified on the basis of
24 combined foraminiferal data from the same section and the relative stratigraphic position of the
25 samples. The stage boundaries are from Gradstein et al. (2012).
26
27
28
29
30
31
32
33
34

35 Figure 9. Correlation diagram of selected Upper Jurassic – Lower Cretaceous strata in the Eastern
36 Black Sea region, highlighting possible common hiatus age ranges and their potential driving
37 mechanisms. The sections are located on Figure 1.
38
39
40
41
42

43 Figure 10. Examples of meteoric dissolution porosity in Late Jurassic carbonates from the Black Sea
44 region. A) Lithoclastic oolitic grainstone from the Late Tithonian Bedeneyr Formation at locality
45 CR35 in central Crimea showing oomouldic secondary porosity (black arrow). B) Reef boundstones
46 from the Late Tithonian Baydar Formation at locality CR54 in southwest Crimea showing dissolution
47 vugs largely filled by differing generations of phreatic cements (black arrow). Sample localities are
48 shown on Figure 1.
49
50
51
52
53
54
55
56
57
58
59
60
61
62
63
64
65

Figure 1 Colour





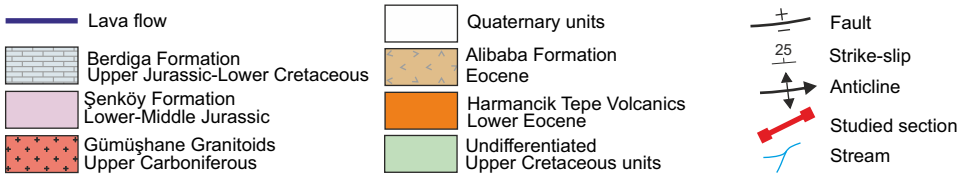
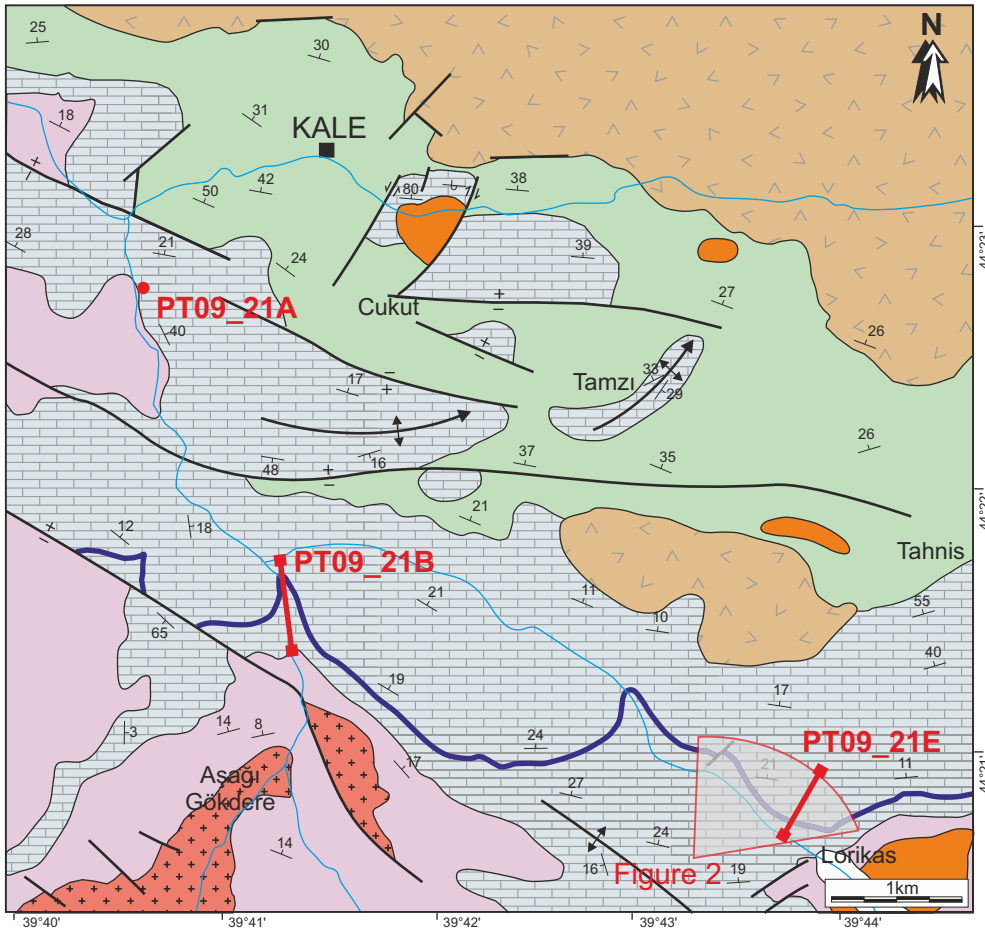


Figure 4 Colour

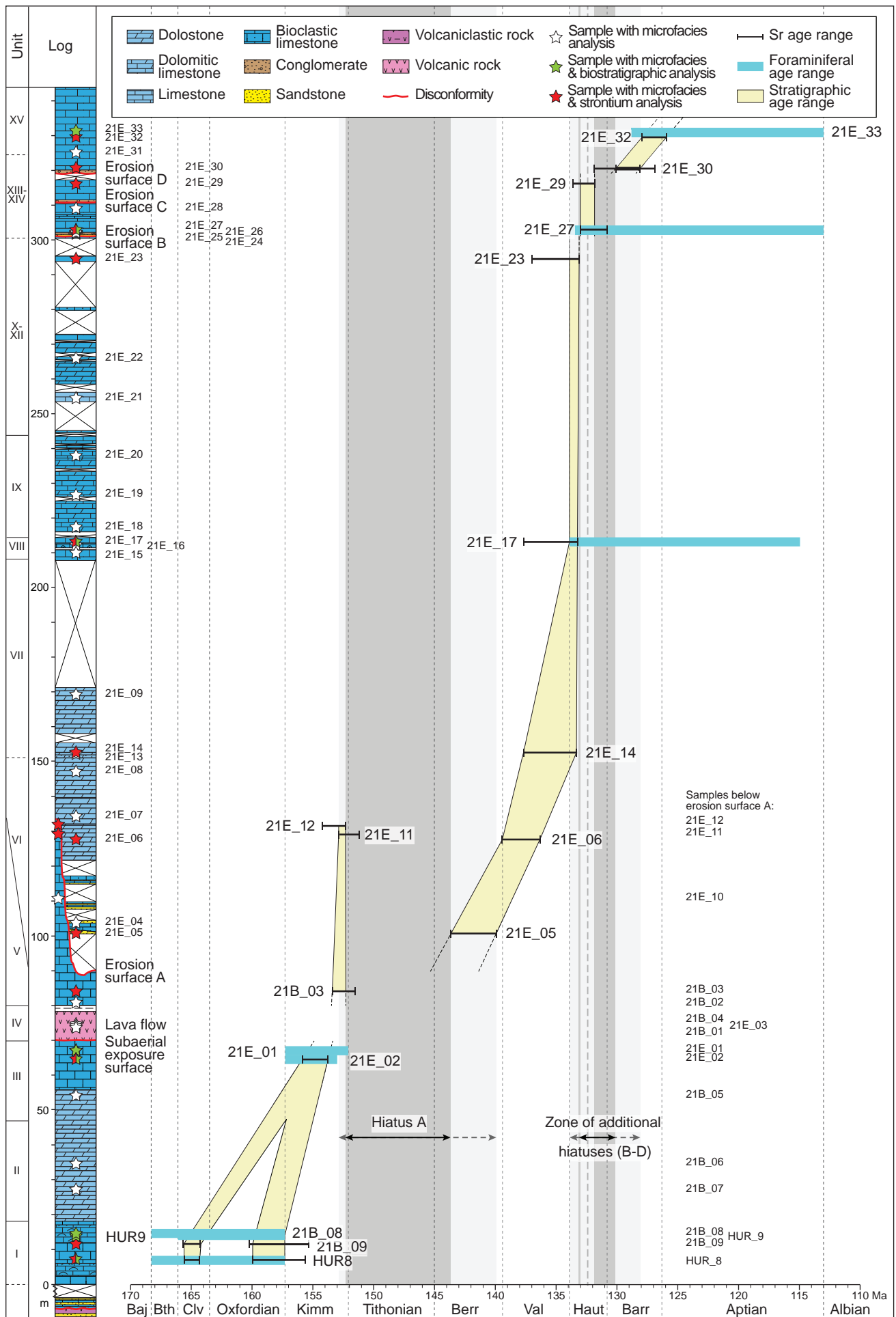


Figure 5 Colour
[Click here to download high resolution image](#)

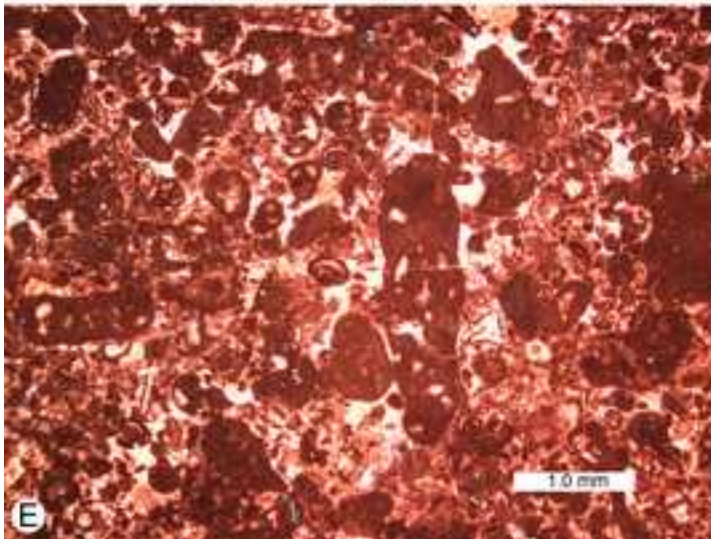
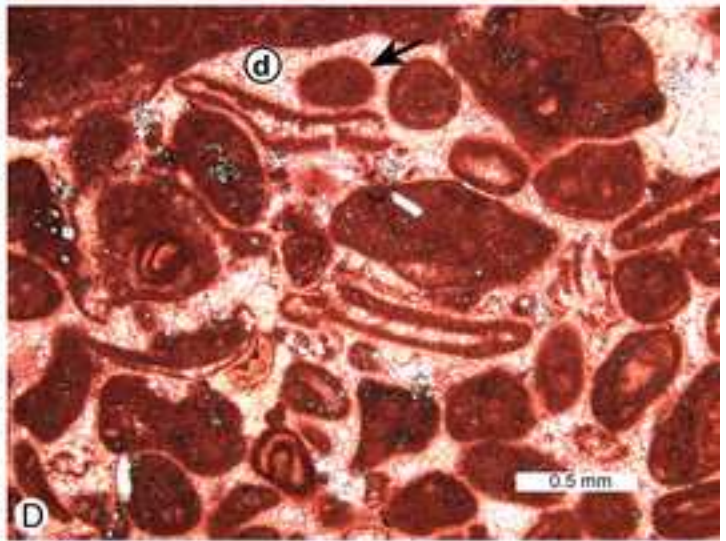
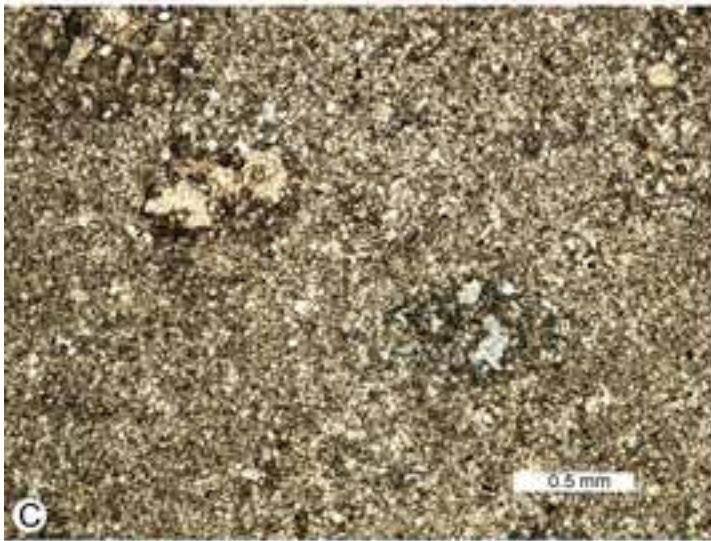
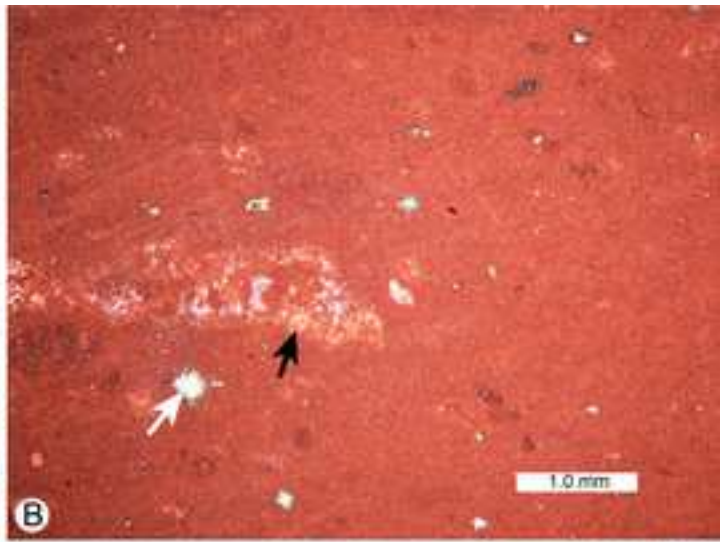
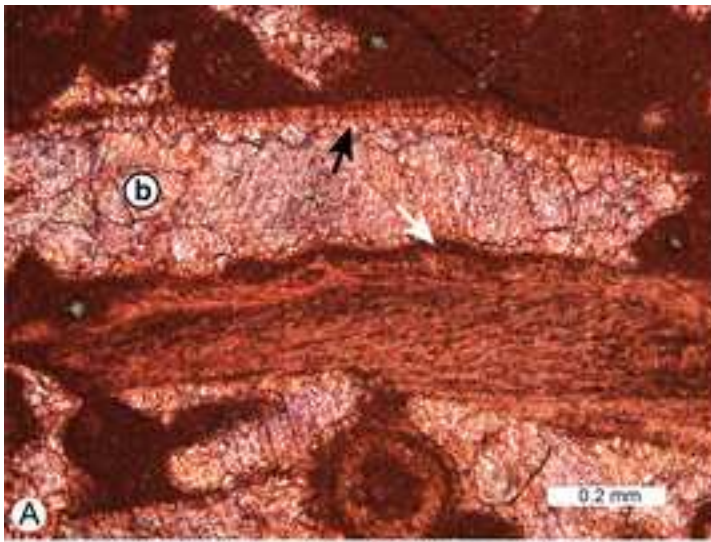
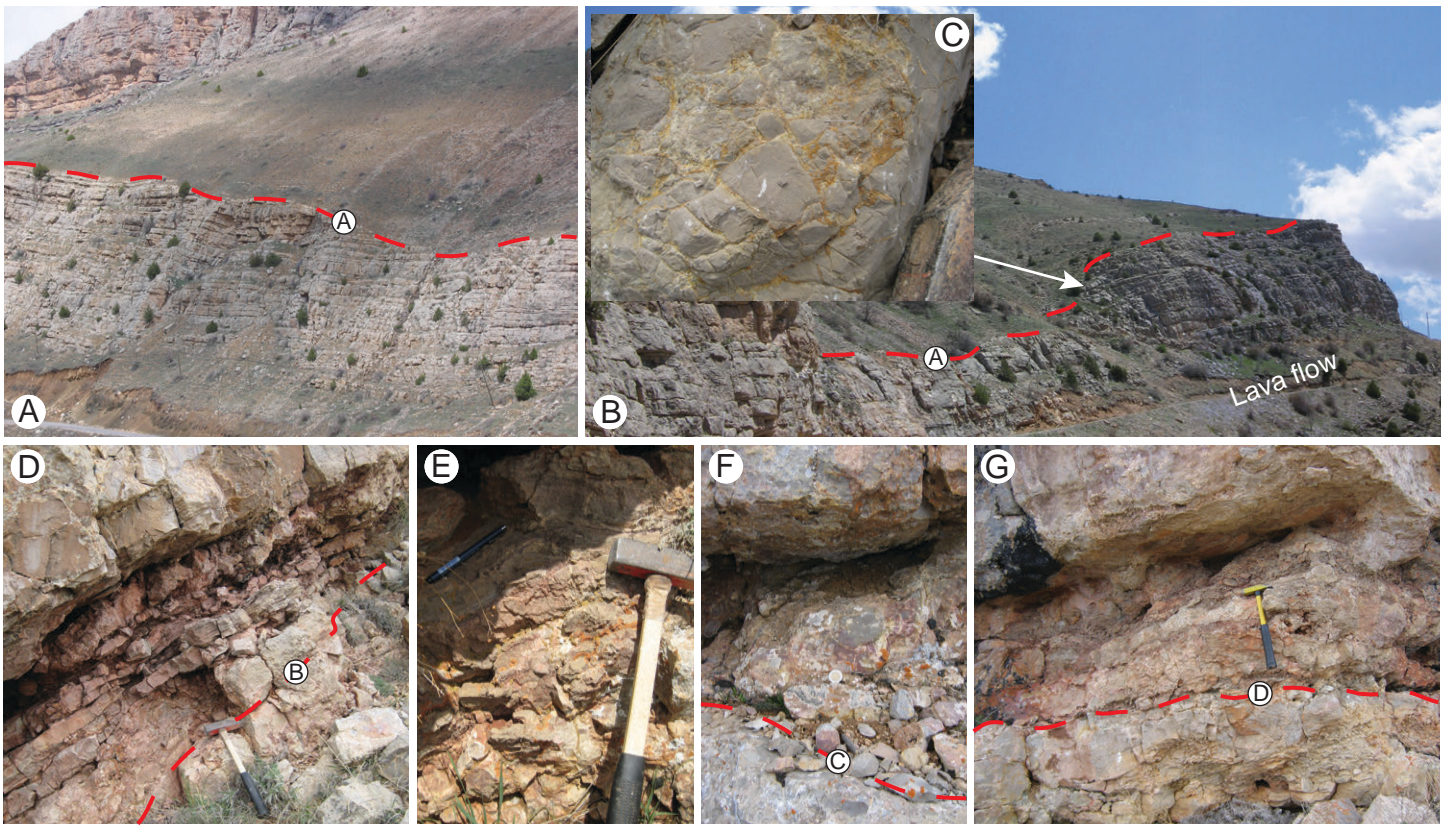


Figure 6 Colour



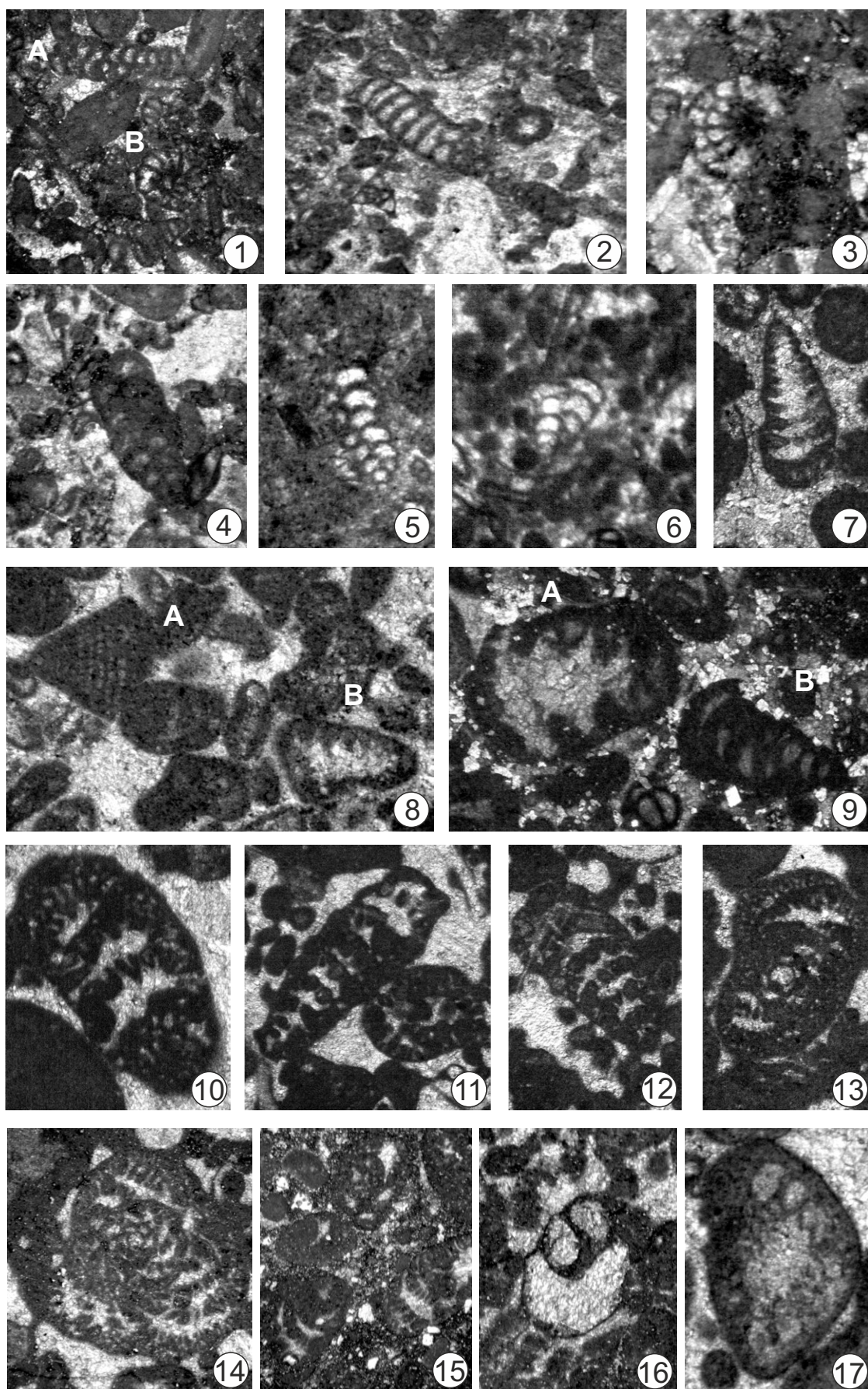


Figure 8 Colour

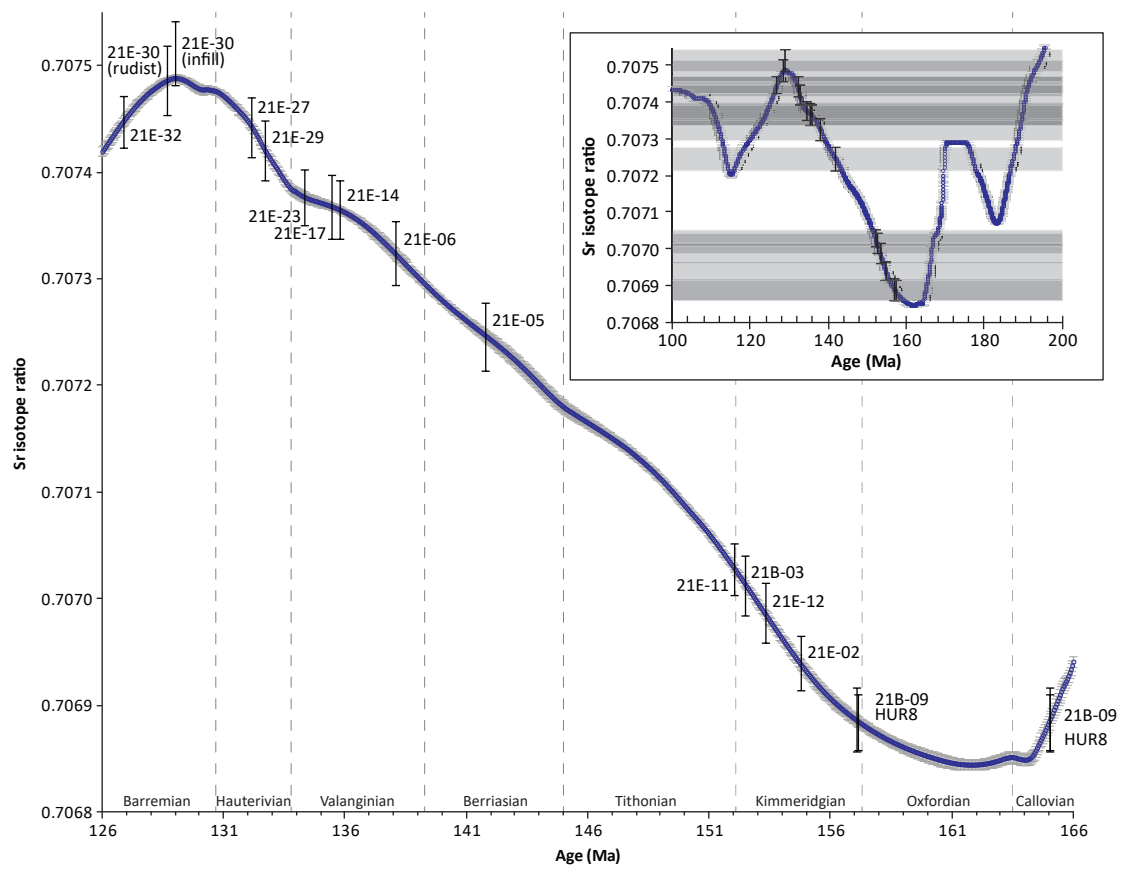


Figure 10 Colour
[Click here to download high resolution image](#)

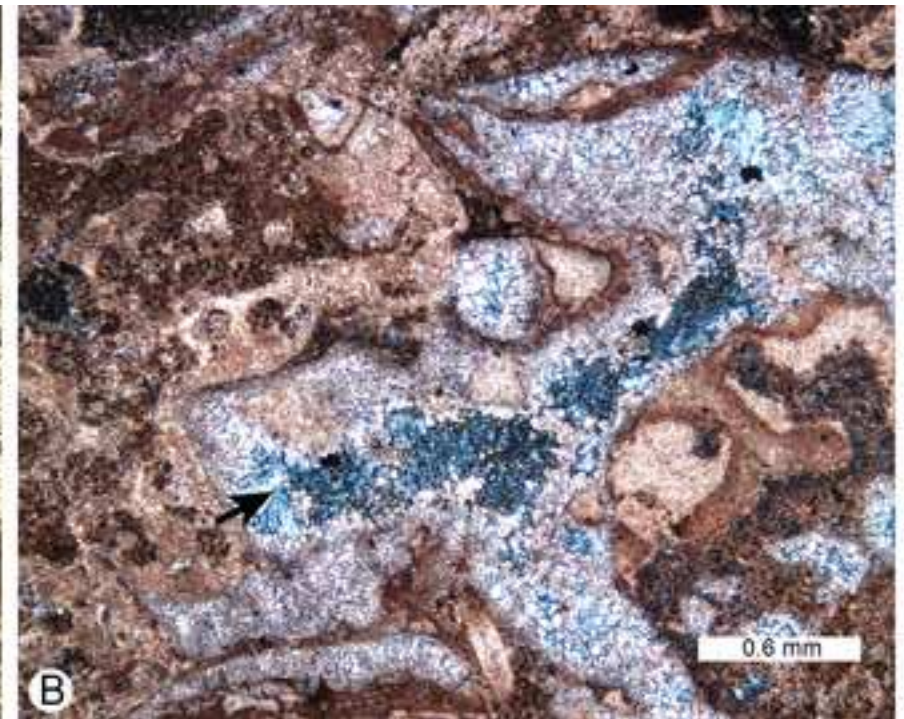
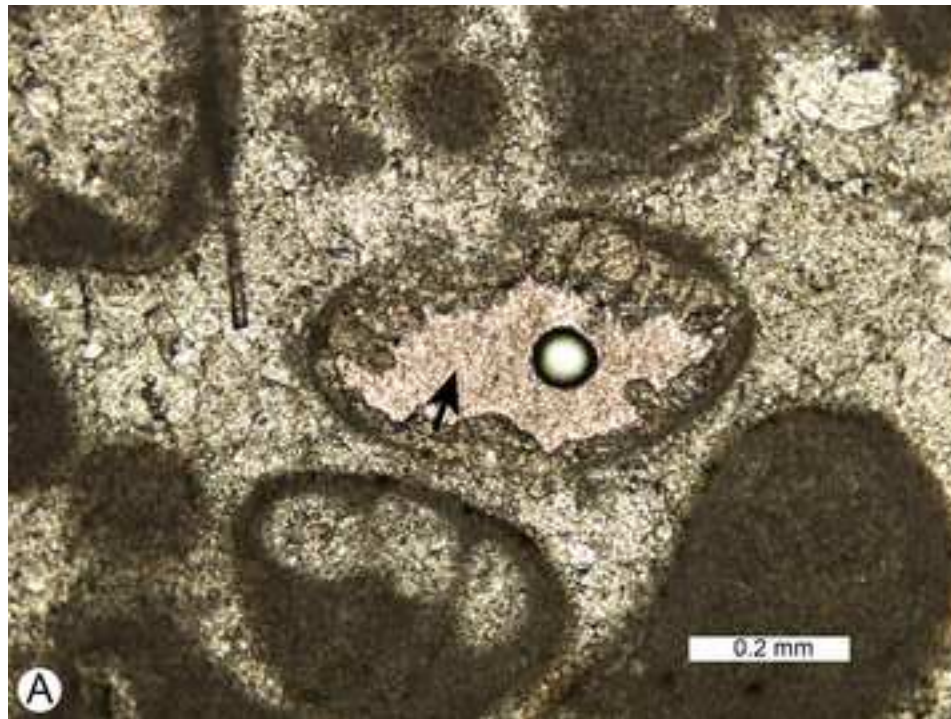


Table 1

Koch et al. (2008)					This work		
Stratigraphic unit	Thickness (m)	Description	Interpretation	Age range	Thickness (m)	Additional comments	Reinterpreted maximum age range
XVI	23	Interbedded intraclastic, foraminiferal wackestones, packstones and grainstones.	Low-energy intertidal to high-energy shallow normal marine conditions.	Barremian		Not observed.	
XV	20	Thick to very thick bedded packstones-grainstones interbedded with medium to thick bedded lime mudstones to wackestones with algal laminations and birdseye structures.	Moderate- to high-energy, shallow to intertidal normal marine conditions.	Hauterivian	>19	Thick bedded bioclastic packstones and grainstones with minor lime mudstone interbeds.	Late Barremian to Early Aptian
XIV	20	Thick bedded intraclastic-foraminiferal-dasycladian packstones-grainstones with four thin intercalated siliciclastic layers containing volcanic rock fragments.	Alternating low- and high-energy normal marine conditions.	Late Valanginian - Early Hauterivian	24	Contains erosion surfaces C & D. Each surface is overlain by reddened breccia-conglomerates (clasts). Clay filled fissures occur below surface C. Other lithologies include sandstone, foraminifera packstone-grainstone, mollusc floatstone, intraclastic and bioclastic grainstone, bioclastic wackestone, lime mudstones and laminated stromatolites.	Early Hauterivian to Late Barremian
XIII	3	Dolomite overlain by a 70 cm thick conglomerate.	Low-energy conditions.	Late Valanginian			
XII	10	Medium to thick bedded intraclastic-foraminiferal-dasycladian packstones-grainstones interbedded with dolomitic limestone and dolomite.	High-energy conditions.	Late Valanginian	57	Medium- to thick-bedded intraclastic and bioclastic wackestones, packstones and grainstones that have undergone varying amounts of dolomitization. Capped by erosion surface B.	Early Hauterivian
XI	12	Medium bedded fine- to medium-crystalline dolomite.	?Low- to moderate-energy conditions.	Early Valanginian			
X	13	Medium to thick bedded, partially dolomitised, gastropod-rich intraclastic-foraminiferal packstones-grainstones.	High-energy conditions.	Earliest Valanginian			
IX	31	Medium to thick bedded, partially dolomitised, intraclastic-foraminiferal packstone-grainstones.	?Low- to moderate-energy conditions.	Berriasian	30	Medium- to thick-bedded, dolomitized bioclastic wackestones.	Early Hauterivian
VIII	4	Medium to thick bedded, dolomitic intraclastic, oolitic and foraminiferal packstones and grainstones.	High-energy (open) shallow-water environment.	Earliest Berriasian	5	Medium- to thick-bedded intraclastic and bioclastic, coated grain packstones and grainstones.	Late Valanginian to Early Hauterivian
VII	36	4 m of in situ fine- to medium-crystalline dolomite. Slope debris composed of micritic limestones.	Low-energy environment.	Latest Tithonian	57	Dolostones	Early Valanginian to Early Hauterivian
VI	30	Medium to thick bedded lime mudstones. The lower 8 m are reported to be Kimmeridgian.	Low-energy, restricted environment.	Latest Kimmeridgian-Tithonian	17-62	Lower 45 m thick incised valley fill (not recognised by Koch <i>et al.</i> , 2008) comprises limestone breccias, conglomerates, sandstones (volcanic lithic arkoses) and dolostones. Valley shoulder sediments comprise thick bedded dolostones.	Early Berriasian to Early Hauterivian
V	43	Thick bedded lime mudstones that are locally brecciated, with local biomicrites.	Low-energy, restricted environment.	Late Kimmeridgian	9-54	Thick bedded lime mudstones. The uppermost sediments are brecciated and karstified and capped by erosion surface A with up to 45 m of local relief.	Late Kimmeridgian
IV	10	Heavily weathered 'diabase sill' that includes single large pillows.	Submarine extrusion.	Middle Kimmeridgian	10	Highly weathered doleritic lava flow. Pillow structures and entrained limestones suggest subaqueous eruption. Capped by tuffaceous siltstones and reddish mudstones deposited in a nearshore to subaerial environment.	?Late Kimmeridgian
III	23	Medium to thick bedded micritic limestones with local algal laminations and only minor biogenic components. Contains reworked volcanic rock fragments and evidence for subaerial exposure.	Restricted platform interior. Contemporaneous volcanic activity.	Late Oxfordian to Early Kimmeridgian	23	Medium to thick bedded dolostones passing up into lime mudstones. Subaerial dissolution surface at top.	Late Oxfordian to Kimmeridgian or Kimmeridgian
II	29	Medium bedded fine- to medium- and thick to very thick bedded medium- to coarse-crystalline dolomites. Ghosts of foraminifera, ooids, oncoids and peloids.	Moderate-energy, more restricted platform conditions.	Middle to Late Oxfordian	29	Medium to thick bedded dolostones.	Callovian to Late Oxfordian or Late Oxfordian to Early Kimmeridgian
I	18	Medium bedded wackestone-packstone and very thick bedded packstone-grainstone interbeds. Microbial oncoids are characteristic. Intraclasts include coral and agglutinated foraminifera.	Moderate- to high-energy, open marine platform conditions.	Early Oxfordian	18	Very thick bedded intraclastic and bioclastic packstones, and grainstones.	Callovian to Early Oxfordian or Middle Oxfordian to earliest Kimmeridgian

Table 2

Sample number	Height (m)	Stratigraphic unit	Biological components	Depositional environment	Determined age
21E_33	331	XV	<i>Arenobulimina</i> sp., miliolid spp., <i>Lituola</i> sp., <i>Pseudolituonella gavonensis</i> , <i>Pseudopfenderina neocomiensis</i> , <i>Vercorsella arenata</i> , <i>Cuneolina laurenti</i> , <i>Debarina hahounerensis</i> , <i>Dasyclad</i> spp. (<i>Cylindroporella</i> sp.)	Low energy restricted environment	Late Barremian - Aptian (Late Barremian based on first occurrence of <i>Debarina</i> sp.)
21E_31	325		Small miliolids, <i>Cuneolina</i> sp., <i>Vercorsella</i> sp., <i>Dasyclad</i> spp. (<i>Cylindroporella</i> sp.)		
21E_30	320.5		Small miliolids		
21E_29	316		Small miliolids, ? <i>Cuneolina</i> sp.		
21E_28	309	XIII-XIV	Small miliolids, <i>Pseudocyclammina</i> sp., <i>Textularia</i> sp., <i>Everticyclammina</i> sp., <i>Everticyclammina virguliana</i>		
21E_27	303		Small miliolids, <i>Pseudocyclammina</i> sp., <i>Textularia</i> sp., <i>Everticyclammina</i> sp., <i>Buccicrenata</i> sp., <i>Praechrysalidina infracretacea</i> , <i>Vercorsella arenata</i> , <i>Pfenderina neocomiensis</i> , <i>Dasyclad</i> spp. (<i>Cylindroporella</i> sp.)		Hauterivian - Aptian (Hauterivian based on the first occurrence of <i>Praechrysalidina infracretacea</i> and <i>Vercorsella arenata</i>)
21E_23	294.5	X-XII	Small miliolids, <i>Textularia</i> sp., <i>Pfenderina</i> spp., <i>Ammobaculites</i> sp., <i>Textularia</i> sp., <i>Buccicrenata</i> sp., <i>Dasyclad</i> spp.		
21E_21	254.5		Small miliolids, <i>Textularia</i> sp.		
21E_20	238		Small miliolids		
21E_19	227	IX	Small miliolids, <i>Textularia</i> sp., <i>Riyadhoides</i> sp. (reworked), <i>Andersenolina elongata</i> , <i>Dasyclad</i> spp., <i>Gastropod</i> spp.		
21E_18	217.5		Small miliolids, <i>Textularia</i> sp., <i>Riyadhoides</i> sp. (reworked), <i>Andersenolina elongata</i> , <i>Dasyclad</i> spp., <i>Gastropod</i> spp.		
21E_17	212.5		Small miliolids, <i>Textularia</i> sp., <i>Riyadhoides</i> sp. (reworked), <i>Everticyclammina</i> sp., <i>Kastamonina abanica</i> (reworked), <i>Andersenolina elongata</i> , <i>Cuneolina camposaurii</i> , <i>Dasyclad</i> spp., <i>Gastropod</i> spp.	Hauterivian - Aptian assemblage based on <i>Cuneolina camposaurii</i>	
21E_16	211.5	VIII	Small miliolids, <i>Textularia</i> sp., <i>Riyadhoides</i> sp., <i>Andersenolina elongata</i> , <i>Praechrysalidina infracretacea</i> , <i>Protpeneroplis</i> sp., <i>Dasyclad</i> sp.	?Kimmeridgian - Tithonian (<i>Riyadhoides</i> a Late Jurassic form but maybe reworked)	
21E_15	209.5		Small miliolids, <i>Textularia</i> sp., <i>Pseudomarssonella</i> sp., <i>Protpeneroplis</i> sp., <i>Pfenderina</i> sp., <i>Andersenolina elongata</i> , <i>Riyadhoides</i> sp., <i>Dasyclad</i> sp.	?Kimmeridgian - Tithonian (<i>Riyadhoides</i> a Late Jurassic form but maybe reworked as above)	
21E_05	101	VI	<i>Dasyclad</i> s algae		
21E_01	67.5		<i>Streptocyclammina parvula</i> , <i>Everticyclammina virguliana</i> , <i>Gastropod</i> spp.	Kimmeridgian	
21E_02	65	III	<i>Alveosepta jaccardi</i> , <i>Pseudocyclammina lituus</i> , <i>P.</i> sp., <i>Rectocyclammina chouberti</i> , <i>Mesoendothyra</i> sp., <i>Everticyclammina</i> sp., <i>Buccicrenata</i> sp., <i>Gastropod</i> spp., <i>Dasyclad</i> spp.	Early - early Late Kimmeridgian	
21B_08	15		<i>Trocholina conica</i> , <i>Neotrocholina</i> sp., <i>Textularia</i> spp., <i>Nautiloculina</i> sp.	Bathonian - Oxfordian	
HUR9	14	I	<i>Trocholina conica</i> , <i>Trocholina</i> cf. <i>solecensis</i>	Callovian-Oxfordian	
HUR8	8		<i>Protpeneroplis striata</i> , <i>Trocholina conica</i> , <i>Neotrocholina</i> sp., <i>Textularia</i> spp., <i>Nautiloculina</i> sp.	Bathonian-Oxfordian	
HUR6	2		Recrystallised algae, ? <i>Protpeneroplis striata</i>	?Bathonian-Berriasian	

Table 3

Sample number	Comment on sample	Height (m)	Stratigraphic unit	Position relative to erosion surfaces	Sr isotope ratio	2 sigma error	Max age (Ma)	Min age (Ma)	Comment on age interpretation
21E_32	difficult to avoid vein	329.5	XV	above D	0.707447	0.000024	127.95	125.95	Several possible ages but only one that is compatible with the overlying foram data and stratigraphic position
21E_30 rudist	rudist	320.5	XIII-XIV	above D	0.707486	0.000032	131.90	126.90	Only the lower error range intersects with the sea level curve
21E_30 infill	micrite infill	320.5		above D	0.707512	0.00003	130.10	128.10	Only the lower error range intersects with the sea level curve
21E_29		316		above D	0.707420	0.000028	133.65	131.85	Several possible ages but only one that is compatible with the foram data and stratigraphic position. Within error of the stratigraphically lower 21E_27, which constrains the ages of both these samples to the area of overlapping errors. Note however, the erosion surface that separates the two.
21E_28		309		between C & D	0.7075283	0.000036			Ages not stratigraphically compatible
21E_27		303		between B & C	0.707442	0.000028	132.80	131.25	Several possible ages but only one that is compatible with the foram data and stratigraphic position. Within error of the stratigraphically higher 21E_29, which constrains the ages of both these samples to the area of overlapping errors. Note however, the erosion surface that separates the two.
21E_23	bivalve	294.5	X-XII	between A & B	0.707377	0.000026	137.00	133.10	Several possible ages but only one that is compatible with the overlying foram data and stratigraphic position
21E_17		212.5	VIII	between A & B	0.707368	0.00003	137.65	133.25	Several possible ages but only one that is compatible with the stratigraphic position and foram data
21E_14		153	VII	between A & B	0.707365	0.000028	137.70	133.35	Several possible ages but only one that is compatible with the stratigraphic position
21E_12		132	V	below A	0.706987	0.000028	154.25	152.35	Two possible ages: the younger is compatible with the foram data below. Within error of the stratigraphically lower 21E_11, which constrains the ages of both these samples to the area of overlapping errors.
21E_11	micrite	129.5		below A	0.707028	0.000024	152.90	151.20	Two possible age ranges. The younger one is compatible with both the foram data below. Within error of the stratigraphically higher 21E_12, which constrains the ages of both these samples to the area of overlapping errors.
21E_06		128	VI	between A & B	0.707324	0.00003	139.45	136.35	Several possible ages but only one that is compatible with the stratigraphic position
21E_05	micrite	101		between A & B	0.707246	0.000032	143.70	139.95	Several possible ages but only one that is compatible with the stratigraphic position
21B_03	Lime mudstone	84.5	V	below A	0.707013	0.000028	153.45	151.50	Two possible age ranges. The younger one is compatible with both the foram data and stratigraphic position
21E_02	brachiopod	65	III	below A	0.706940	0.000026	155.90	153.80	Two possible age ranges. The younger one is compatible with both the foram data and stratigraphic position
21B_08	difficult to avoid vein	15	I	below A	0.707528	0.000028			Not stratigraphically compatible; probably diagenetically altered as a result of vein carbonate
HUR9		14		below A	0.707857	0.000028			Ages not stratigraphically compatible
21B_09		12		below A	0.706887	0.00003	160.25	155.35	Two possibilities due to inflection point in the seawater curve
				below A	0.706887	0.00003	165.70	164.25	
HUR8		8		base of section	0.706885	0.000026	159.95	155.60	Two possibilities due to inflection point in the seawater curve
			base of section	0.706885	0.000026	165.60	164.30		

Table 4

Sample number	Height (m)	Biological components	Determined age
17_16	111.5	<i>Pseudocyclammina lituus</i>	Callovian-Tithonian (Kimmeridgian-Tithonian because of underlying sample)
17_15	108.5	<i>Pseudocyclammina lituus</i> , <i>Pseudocyclammina</i> sp., <i>Everticyclammina</i> sp., <i>Cladocoropsis mirabilis</i>	Kimmeridgian-Tithonian
17_14	102.5	<i>Cladocoropsis mirabilis</i>	Callovian-Tithonian (Kimmeridgian-Tithonian because of underlying sample)
17_13	95.5	<i>Pseudocyclammina lituus</i>	Callovian-Tithonian (Kimmeridgian-Tithonian because of underlying sample)
17_12	89	<i>Cladocoropsis mirabilis</i>	Callovian-Tithonian (Kimmeridgian-Tithonian because of underlying sample)
17_11	84	<i>Pseudocyclammina lituus</i>	Kimmeridgian - Tithonian (because of underlying sample)
17_10	80	<i>Batcinella</i> sp., <i>Actinoporella podolica</i> , <i>Andersenolina alpina</i>	Callovian-Tithonian (Kimmeridgian-Tithonian because of underlying sample)
17_08	74	<i>Cladocoropsis mirabilis</i>	Callovian-Tithonian (Kimmeridgian-Tithonian because of underlying sample)
17_07	68	<i>Actinoporella podolica</i> , <i>Cladocoropsis mirabilis</i>	Callovian-Tithonian (Kimmeridgian-Tithonian because of underlying sample)
17_06	66	<i>Pseudocyclammina lituus</i>	Callovian-Tithonian (Kimmeridgian-Tithonian because of underlying sample)
17_04	49.5	Dasyclad algae <i>Actinoporella podolica</i> , <i>Triploporella</i> spp., <i>Paleodasyclads</i> sp., miliolid spp., <i>Nautiloculina oolithica</i> , <i>Pseudocyclammina lituus</i> , <i>Everticyclammina</i> sp., <i>Pseudocyclammina bukowiensis</i>	Kimmeridgian
17_03	47	Dasyclad algae <i>Triploporella</i> spp., miliolid spp., <i>Nautiloculina oolithica</i> , <i>Pseudocyclammina lituus</i>	Kimmeridgian (because of overlying samples)
17_02	38	Dasyclad algae <i>Triploporella</i> spp., miliolid spp., gastropod spp., <i>Buccicrenata primitiva</i>	Kimmeridgian
17_01	36	Dasyclad algae <i>Triploporella</i> spp., gastropod spp., <i>Buccicrenata primitiva</i>	Kimmeridgian